STRUCTURAL ANALYSIS ALONG THE GRENVILLE FRONT NEAR SUDBURY, ONTARIO

STRUCTURAL ANALYSIS ALONG THE GRENVILLE FRONT NEAR SUDBURY, ONTARIO

By

MAO-YANG HSU, B. Sc.

A Thesis

Submitted to the Faculty of Graduate Studies

in Partial Fulfilment of the Requirements

for the Degree

Master of Science

McMaster University

July, 1968

MASTER OF SCIENCE (1968) McMaster University
(Geology) Hamilton, Ontario

TITLE: Structural Analysis along the Grenville Front near Sudbury, Ontario

AUTHOR: Mao-Yang Hsu, B.Sc. (National Taiwan University)

SUPERVISOR: Professor P.M. Clifford

NUMBER OF PAGES: ix, 104.

SCOPE AND CONTENTS:

A region across the Chief Lake batholith and the Grenville province near Sudbury was mapped, described, and structurally analysed.

Rock specimens were sectioned to provide additional data bearing on the metamorphic petrology.

Both macroscopic and mesoscopic folds were subjected to detailed geometric analysis. Four different types of folds were found. The geometries of different tectonite fabrics were compared to the deformation ellipsoid. Homogeneous and heterogeneous deformations are discussed. Finally, tectonic synthesis was used to interpret the successive sequence of geologic events and tectonite fabrics.

ABSTRACT

Amphibolites and gneisses of the "Grenville province" and granitic rocks of the Chief Lake batholith near Sudbury show the effects of several phases of deformation.

The first phase of deformation affected previously metamorphosed rocks of the "Grenville province" together with enclosed pegmatite sills, and formed congruous parasitic S- and Z-folds. The rocks were then subjected to faulting and local refolding. About 1,750 m.y. ago, the Chief Lake batholith was intruded and truncated the previous folds. Finally, all the rocks were subjected to a simultaneous regional metamorphism and strong deformation.

During this final deformation, all the previous linear structures were rotated to parallel the strongly-developed regional mineral lineations. The high-grade rocks of high amphibolite facies to the S.E. of the cataclastic zone flowed upwards from a greater depth than the rocks of greenschist facies to the N.E. of the cataclastic zone. The sharp increase in metamorphic grade occurs within the cataclastic zone which is about one mile wide.

The final progressive deformation of the rocks is compared with the constant-volume deformation ellipsoid as initiated from the uniaxial prolate type through the constriction type to the plane-strain type; wherein the direction of maximum elongation plunges moderately to the S.S.E. and parallels the regional mineral lineations, the passive fold axes, the elongations of conical folds, and the original flow directions (shown by deformed mineral lineations) of slip folds; while the direction of maximum shortening generally plunges to the N.W. and is normal to the penetrative foliations and the active axial planes of slip folds.

ACKNOWLEDGMENTS

Thanks are expressed to Professor P.M. Clifford for his suggestion and supervision of the research. David Orr's assistance in the field for nine days is very much appreciated. The writer has been helped by discussion with his fellow graduate students Roger J. Rector and Douglas Underhill. Special thanks are due to Dr. J.R. Henderson, the pioneer of structural studies in the neighbouring area, who helped the writer at the beginning of the field work, suggested references to read, and finally gave constructive criticism of this thesis.

Financial assistance towards this study was received from the Ontario Department of University affairs, the Geological Survey of Canada, the National Research Council of Canada, and McMaster University.

TABLE OF CONTENTS

LIST OF FIGURES

CHAPTER 1

INTRODUCTION

The Grenville "front" is the northwestern boundary of the Grenville province in the Canadian Precambrian shield (Stockwell, 1964). It is a major tectonic feature of the earth, extending for more than 1,800 kilometers, across the Canadian shield from Georgian Bay on Lake Huron in the southwest to the coast of Labrador in the northeast. The rocks on both sides of the "front" differ in structure and in grade and age of major metamorphism, and have been relatively well-defined. However, the nature of the boundary between the two sides remains a major problem. Many previous geological studies along the front show discrepancies in interpretation of the nature of the boundary. The map area along the Grenville front near Sudbury was chosen for structural analysis in order to provide an understanding of the front.

I. LOCATION AND COMMUNICATION

The map area is situated ten kilometers south-southeast of Sudbury, Ontario (Figure 1). The juncture of four townships - Broder, Dill, Tilton, and Secord - is located in the southwestern portion of the map area which encompasses an area of approximately 25 square kilo-

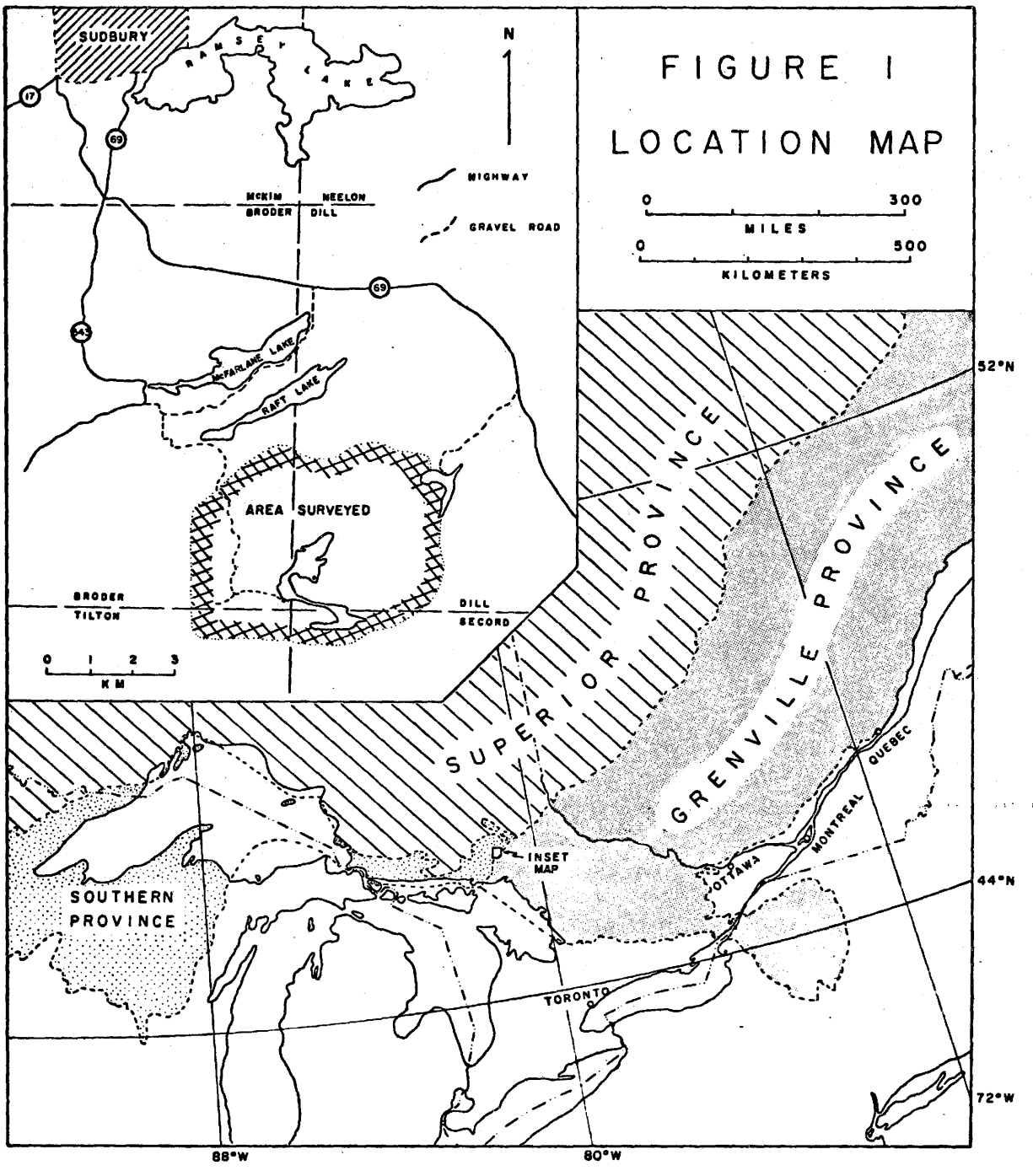
FIGURE 1
LOCATION MAP
0 300
MILES
0 500
KILOMETERS
N
HIGHWAY
GRAVEL ROAD
SUDBURY
RAMSEY LAKE
McKIM
BRODER
NEELON
DILL
McFARLANE LAKE
RAFT LAKE
AREA SURVEYED
BRODER
TILTON
DILL
SECORD
0 1 2 3
KM
SUPERIOR PROVINCE
GRENVILLE PROVINCE
SOUTHERN PROVINCE
INSET MAP
OTTAWA
MONTREAL
QUEBEC
TORONTO
52°N
44°N
72°W
88°W
80°W

meters. One gravel road branching from Route 543 runs across the western border of the area, and another gravel road connects Dill Lake, located at the northeastern corner of the area mapped, with Highway 69.

The map area is included in the topographic map of Coniston (NTS Sheet 41 $^{I}/_{7}$ west) on a scale of 1:50,000. Enlarged aerial photographs, on a scale of approximately 12 inches to one mile (1:5,280), were used in the field. The final geologic map as shown on Figure 2 is reduced to a scale of 4 inches to one mile (1:15,840).

II. PREVIOUS WORK

The regional geology of about four-fifths of the western portion of the map area under investigation was first mapped by Grant et al. (1962), whereas one fifth of the area on the southeast remained unmapped geologically until the writer began field work in May of 1967.

CHAPTER 2

PETROGRAPHY

The rocks in the map area are divided into two major lithologic units - Chief Lake batholith (Henderson, 1967) and Grenville province rocks. The Chief Lake batholith contains granitic rocks whereas the Grenville province rocks include high-grade metamorphic rocks such as amphibolite and gneisses. Besides the two major lithologic units, minor diabase dikes occur as small intrusive bodies.

I. CHIEF LAKE BATHOLITH ROCKS

General Relationships

The Chief Lake batholith occupies one third of the map area (Figure 2), covering about 8.5 square kilometers. The batholith rocks extend northeast and wedge out in southern Neelon Township. The southern limit of the batholith is not certain, but it is believed that the batholith may be the north extension of the Killarney batholith mapped by Quirke and Collins (1930).

The northwestern boundary of the batholith is beyond the map area, but according to Henderson (1967), the contact between the batholith and the Southern province rocks near the map area is marked by a hornblende metagabbro and is very sharp. On the other hand, the contact between the batholith and the Grenville province rocks in the map area is gradational. In the southwestern part of the map area, a migmatite zone occurs along the southeastern border of the batholith (Figure 2). The migmatite is a foliated and lineated mixture of batholithic and country rocks. The country rock is mostly layered quartzofeldspathic gneiss with minor amphibolite belonging to the Grenville province rocks. The migmatite grades northwestward into blastoporphyritic adamellite, and grades southeastward into gneisses and banded amphibolites.

North of the migmatitic rock, feldspathic quartzite is the most common inclusion found in the batholith. Others are amphibolite, gabbro, dark gneiss, and metagreywacke in decreasing order of abundance. The xenoliths generally show a preferred orientation, with their longest dimension subparallel to the strike of penetrative foliation which transects both the batholith and the xenolith. This preferred orientation is common for all types of xenolith rocks in the batholith, but not without exceptions. Some oblong xenoliths of quartzite trend at a large

angle or even normal to the penetrative foliation. The borders of the xenoliths are rarely sharp.

North of the migmatitic gneiss, the batholith is in contact with amphibolite. The contact trends northeast and extends beyond the map area. Although no outcrop of the contact between the batholith and amphibolite was ever observed, the dominantly pink blastoporphyritic rocks (batholith) can be distinguished easily from the dark green amphibolite (Grenville province), and thus a line dividing the two lithologic units is drawn. In the vicinity of the batholith contact, some amphibolite xenoliths apparently are stoped remnants of nearby amphibolite layers. On the other hand, isolated lenses and irregular dikes of pink quartz monzonite were found within the massive or layered amphibolite in the Grenville province.

Texture

In general, the batholithic rocks are foliated and lineated. Foliation is produced by mutually parallel platy minerals such as mica, and lineation is developed by parallel alignment of linear minerals such as quartz and hornblende in recrystallized aggregates. Foliation and lineation are the result of post-intrusion deformation which has modified the primary igneous textures to produce gneissic and blastoporphyritic textures, especially in the portion close to the Grenville province rocks.

Rocks in a larger portion northwest of the batholith, however, show mylonitic or blastomylonitic texture with porphyroblasts of microcline separated by a fine-grained matrix of comminuted feldspar and recrystallized quartz. The feldspar porphyroblasts are commonly fractured and are believed to have survived granulation during the dynamothermal metamorphism. This portion of the batholith is called the "cataclastic zone" (Figure 2).

Mineral Composition

The mineral composition of the Chief Lake batholith in the map area shows that the rock varies from granite to quartz monzonite. Modal analyses of three specimens are listed in Table I. However, Henderson (1967) studied the same batholith in a larger area to the southwest of the map area and found that the rock varies from quartz diorite to quartz monzonite.

Table I. Modal analysis of batholith rocks

Specimen	Qtz	Plag	K-spar	Bio	Mus	Apa	Sphene	Total counts
M60	20	23	28	27	-	1	tr.	600 (biotite adamellite)
T59	27	12	54	6	-	tr.	tr.	600 (granite)
T71	41	6	48	3	tr.	-	-	600 (granite)

In some places, the batholith rock is dark brownish gray and contains up to 20 percent hornblende, 20 percent biotite, and less than 10 percent quartz. These rocks may be the result of assimilation of basic rocks by the magma.

The pinkish gray variety is the major rock of the batholith, and contains more than 90 percent felsic minerals such as quartz, microcline, and plagioclase. Quartz content ranges from 20 to 40 percent, whereas feldspar content is variable (since the texture of the rock makes sampling of porphyroblasts difficult). Consequently, the batholithic rocks vary in composition from quartz diorite to potassic granite.

II. GRENVILLE PROVINCE ROCKS

The grenville structural province in the map area contains high grade metamorphic rocks which are divided into four major lithologies: 1) amphibolite, 2) K-feldspar gneiss, 3) biotite-quartz-feldspar gneiss, and 4) migmatitic quartzo-feldspathic gneiss. Minor lithologies include quartz-biotite-feldspar gneiss, pegmatite, and mica schists.

Although the outcrops of the various kinds of rock in the map area were carefully traced, the stratigraphic succession of the high-grade metamorphic rocks could not be determined. The sequence of Grenville

province map units in the text and on Figure 2 is made in decreasing order of distribution area.

Amphibolite

Amphibolite constitutes about 40 percent of the high-grade metamorphic rock mapped. Most of these amphibolites are layered, with thin quartz-feldspar layers and thick amphibole-rich layers. Some occur as narrow discontinuous lenses in grayish-white gneiss. A massive amphibolite west of Brodill Lake, immediately north of the migmatite zone, contains a small outcrop of diopside amphibolite. Garnet occurs in all amphibolites except this massive body and those intercalated in migmatitic quartzo-feldspathic gneiss.

In general, amphibolite is a dark green to black rock composed essentially of hornblende and plagioclase. Biotite, quartz, garnet, sphene, and apatite may be present as accessory minerals.

Biotite amphibolite is distinguished from common amphibolite by poor gneissosity and field occurrence. At least half of the biotite amphibolite is regarded as ortho-amphibolite which intruded into the apparently para-amphibolite. Evidence for this is shown in Plate 1. Modal analyses of amphibolite specimens (Table II) show that biotite amphibolite contains more than 10 percent biotite whereas common amphibolite has less than 5 percent biotite.

Plate 1

(a) Biotite amphibolite (light-colored outcrop) intruded into foliated quartz-bearing amphibolite. Approximately 320 meters north of the north shore of Brodill Lake.

(b) Stoped remnant of quartz-bearing amphibolite (finer grained) in biotite amphibolite (coarser grained) showing the intrusive relation of the former by the latter. Locality is the same as that for (a).

(a)

(b)

Gneissosity, foliation, and lineation are not conspicuous in biotite amphibolite which is commonly medium- or medium- to coarse-grained*, homogeneous without alignment of biotite. Hornblende content in this rock type ranges from 40 to 60 percent, plagioclase from 25 to 45 percent, biotite from 11 to 19 percent, and quartz from zero to 15 percent.

Common amphibolite contains 40 to 90 percent of hornblende and 28 to 48 percent of plagioclase. This rock type is generally well-banded with foliation and lineation. The foliation is caused by alignment of hornblende and biotite. Common amphibolite may be coarse-, or medium-, or fine-grained, but no trend of grain-size variation relative to geographical position was found. From the combined data of quartz content, well-banded structure and structurally conformable sheets and layers, the common amphibolite is likely to be para-amphibolite, whereas the irregular-shaped bodies of biotite amphibolite lacking mineral orientation are probably, or at least in part, ortho-amphibolite.

---

* Terms of grain size are the same as those applied to igneous rock.

Table II. Modal analysis of amphibolites

Specimen	Hbd	Plag	K-spar	Qtz	Bio	Gnt	Diop	Sil	Sph	Apa	Total Counts
1	51	48	-	-	-	-	-	-	-	-	500
2	54	46	-	-	-	-	-	-	-	-	500
3	40	32	10	15	-	2	-	-	-	1	500
8	58	38	-	-	4	-	-	tr.	-	-	600
15	90	8	-	2	-	-	-	-	-	tr.	600
16	47	38	-	14	-	-	-	-	1	-	600
18	42	32	15	11	-	-	-	-	-	-	500
23	51	38	10	-	-	-	-	-	-	-	500
27	53	47	-	-	-	-	-	-	-	-	500
28	72	28	-	-	-	-	-	-	-	-	500
6*	57	31	-	-	11	-	-	tr.	-	-	600
19*	40	41	-	-	19	-	-	-	-	-	600
25*	48	38	-	-	14	-	-	-	-	-	500
33A*	44	25	-	15	16	-	-	-	-	-	600
59*	40	45	-	-	15	-	-	-	-	-	600
58**	51	34	-	-	-	-	15	-	-	-	600

* Biotite amphibolite

** Diopside amphibolite

K-feldspar Gneiss

Pink K-feldspar gneiss occurs in the northeastern portion of the map area. This rock type is composed essentially of potash feldspar and quartz (Table III). The range of mineral composition is 16 to 49 percent quartz, 43 to 64 percent potash feldspar, 4 to 12 percent plagioclase, 3 to 9 percent biotite, and zero to 4 percent hornblende. No garnet was observed in this pink K-feldspar gneiss.

Many of the rocks show a well-defined planar fabric formed by alternating concentrations of dark and light minerals, and by variations in grain size or by concentrations of pink feldspar and gray quartz into layers. In some varieties, segregation layering is pronounced and may be either between felsic and mafic layers or between coarse K-feldspar layers and finer quartzo-feldspathic layers. These varieties

Table III. Modal analyses of K-feldspar gneiss

Specimen	K-spar	Plag	Qtz	Bio	Hbd	Sph	Apa	Total Counts
T48	45	7	34	9	4	tr.	tr.	500
T50	55	-	39	6	-	-	-	500
T53	54	5	35	5	-	-	-	500
T54	51	4	41	3.5	-	-	-	500
T56	43	-	49	6	2	tr.	tr.	500
T74	64	12	16	7	1	tr.	tr.	500
T75	55	5	36	4	-	-	-	500

can thus be called laminated gneiss.

Structurally discordant relationships of the K-feldspar gneiss, either large- or small-scale, to the surrounding rocks (amphibolite) and preponderance of potash feldspar over quartz may favor an igneous origin.

Biotite-quartz-feldspar Gneiss

Grayish-white biotite-quartz-feldspar gneiss occurs in the southeastern portion of the map area. The visual estimates of mineral composition of the rock are 10 to 35 percent quartz, 15 to 50 percent plagioclase, 10 to 30 percent orthoclase, 8 to 20 percent biotite, zero to 14 percent garnet, and traces of sillimanite, sphene, and apatite.

The grayish-white gneiss has an appearance of "banded (layered) arkose". Grain size of this gneiss ranges from fine to medium. Gradations of this gneiss into feldspathic quartzite were observed in the field and thus a sedimentary origin may be assigned to the grayish-white biotite-quartz-feldspar gneiss.

Another variety of biotite-quartz-feldspar gneiss, such as the one occurring as a xenolith in the batholith about one kilometer northeast of Kasten's farm (Figure 2), contains 15 to 40 percent quartz, 10 to 50 percent potash feldspar, 5 to 30 percent plagioclase, 5 to 20 percent biotite, zero to 25 percent hornblende, zero to 4 percent garnet, and traces of muscovite, sphene, and apatite. This kind of gneiss looks like metagraywacke and is dirty, dark gray, mostly very fine-grained,

and rather friable as compared to the quartzo-feldspathic gneiss. Some varieties contain a high content of microcline which occurs as metacrysts in a dark, dirty, more or less schistose matrix. Pink potash feldspar in the dark rock may be the result of metasomatism, developed under the influence of alkaline granitizing fluids.

Migmatitic Quartzo-feldspathic Gneiss

As has been mentioned before, migmatitic gneiss occurs in the southwestern part of the map area. It is mostly layered quartzo-feldspathic gneiss with minor amphibolite, which was intruded by batholith rocks. Neither sillimanite nor garnet was observed in this rock. Interbeds of paragneiss and amphibolite occur in the western portion of this migmatitic rock.

Quartz-biotite-feldspar Gneiss

This unit occurs as discontinuous, thick layers which are always very closely associated with pink K-feldspar gneiss. The quartz-biotite-feldspar gneiss contains about 15 percent quartz, 20 percent microcline, 25 to 32 percent plagioclase, 20 percent biotite, 5 to 15 percent garnet and traces of apatite (all are visual estimates). The rock is dark-colored, medium-grained, and shows poorly-defined foliation and lineation. Biotite flakes are randomly oriented. At one locality one kilometer west-southwest of Dill Lake, the dark quartz-

biotite-feldspar gneiss was found intruding into the pink K-feldspar gneiss on small scale (Plate 2), although the extension of the intrusion body is parallel to the gneissosity of the surrounding pink gneiss (Figure 2).

Pegmatite

Pegmatites occur as discontinuous lenses in amphibolite or K-feldspar gneiss. Their contacts are commonly subparallel to the gneissosity of amphibolite or gneiss. These pegmatites are composed chiefly of fractured potash feldspar with crystals up to 30 centimeters long. Quartz is a minor constituent. Muscovite, biotite, and garnet are present also in places. Most pegmatites are crudely foliated, with thick folia and rough surfaces due to preponderance of quartzo-feldspathic minerals over other flaky components.

Mica Schist

Mica schist includes muscovite schist, biotite schist, and muscovite-biotite schist. Other minerals present in the rock may include quartz, plagioclase, orthoclase, microcline, garnet, sillimanite, hornblende, sphene, and apatite.

Mica schist is markedly foliated, although the regularity of the foliation tends to be interrupted by the presence of large porphyroblasts of garnet and potash feldspar. The texture is schistose, fine- to medium-grained. Development of porphyroblasts of potash feld-

Plate 2

K-feldspar gneiss (on the left side, light color) intruded by dark quartz-biotite-feldspar gneiss. Approximately one kilometer west-southwest of Dill Lake.

spar is especially common at the places close to the batholith, where alkalies might have been introduced from the nearby granitic rocks.

III. DIABASE DIKES

Small dikes of diabase intrude both batholith and Grenville province rocks. The largest diabase body is in the migmatite zone in the southwestern part of the map area, and is about 40 meters wide and extends for a length of 230 meters. This diabase dike cuts the migmatitic gneiss at an angle of about 30 degrees to the gneissosity.

Diabase is dark olive green and fine- or fine- to medium-grained. In thin section it contains essential plagioclase and clinopyroxene with accessory hornblende. The texture is ophitic with idiomorphic plagioclase enclosed by mafic minerals.

CHAPTER 3

METAMORPHIC GEOLOGY

The area is divided into two metamorphic zones - a biotite zone and a garnet-sillimanite zone - as indicated by the corresponding mineral assemblages developed regionally. The first appearance of sillimanite (observed in thin section only) in pelitic mica-schist xenolith within the batholith - the sillimanite isograd - marks the boundary between the two zones. This sillimanite isograd lies approximately in the middle of the batholith in the map area, and happens to be the boundary between the cataclastic zone and the completely recrystallized area (Figure 3).

Mineral assemblages in the biotite zone are of the green-schist facies of regional metamorphism while in the garnet-sillimanite zone certain diagnostic mineral assemblages indicate that the rocks have undergone a high-grade regional metamorphism under P-T conditions of the amphibolite facies (Hietanen, 1967).

Some xenoliths in the batholith within the garnet-sillimanite zone, including amphibolite and mica schist, contain muscovite and sillimanite (observable only in thin section). Porphyroblasts of

Figure 4

ACF and A'KF diagrams of metamorphic mineral paragenesis.

(a) Muscovite-biotite subfacies of the greenschist facies. Quartz and plagioclase are possible additional phases for ACF diagram. A'KF diagram for rocks with excess SiO_2 and Al_2O_3.

(b) Sillimanite-muscovite subfacies of the amphibolite facies. Quartz and potash feldspar are possible additional phases for ACF diagram whereas quartz and plagioclase are possible additional phases for A'KF diagram.

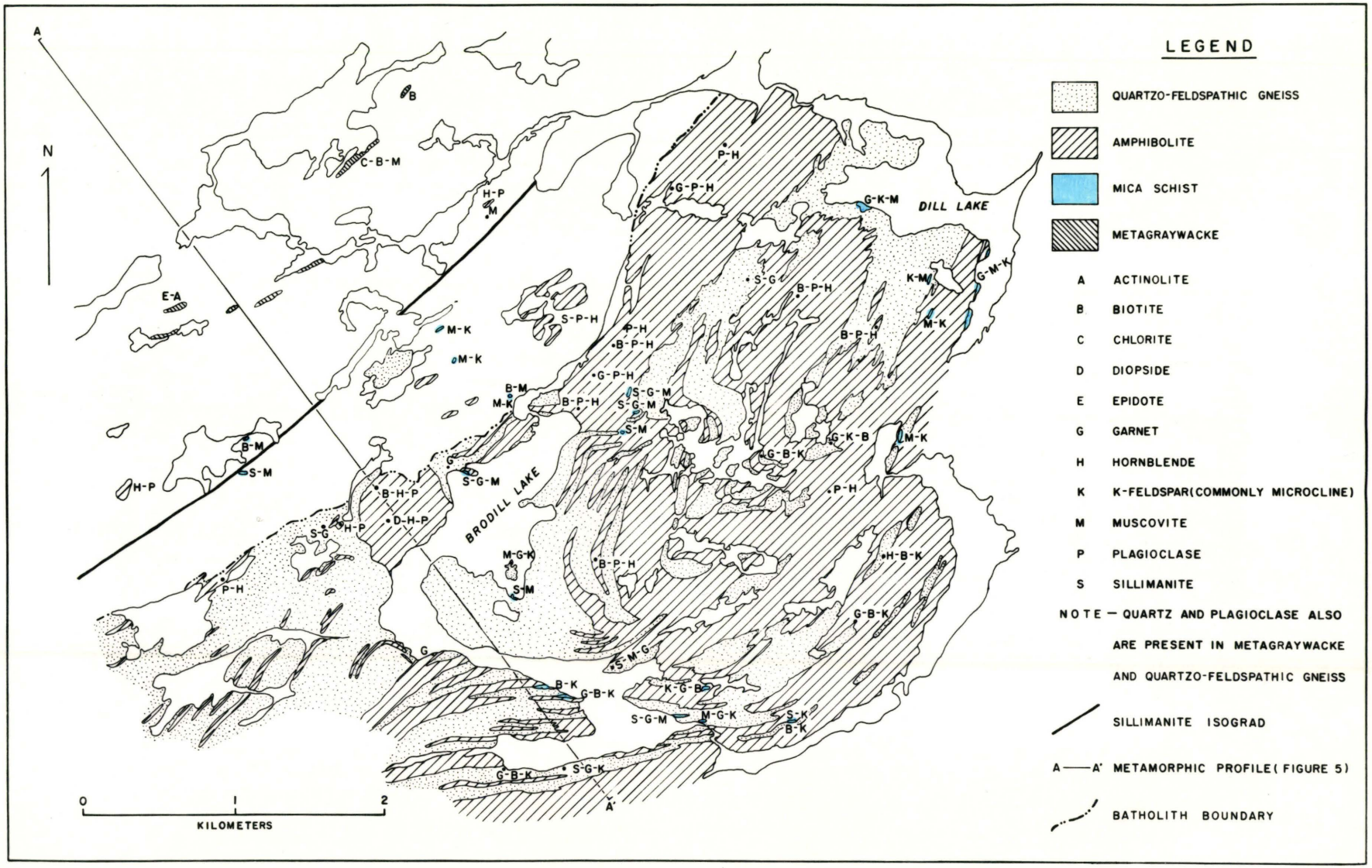

Figure 3. Metamorphic Geology

garnet or microcline are common in the gneissic rocks in the garnet-sillimanite zone. Garnet and sillimanite were found throughout the Grenville province rocks in the map area except the southwestern portion where rocks are massive amphibolite and migmatitic gneiss.

All mafic rocks in the garnet-sillimanite zone contain plagioclase and amphibole; some minor quartz and biotite may be present also. Amphibole is actinolite or hornblende in the biotite zone, but only hornblende in the garnet-sillimanite zone. Chlorite and epidote are only in the biotite zone. Diopside amphibolite only occurs as a small lenticular body in the massive amphibolite west of Brodill Lake.

I. BIOTITE ZONE

For convenience, the rocks northwest of the sillimanite isograd in the map area are all placed in the biotite zone, in which biotite is widely distributed in all quartzo-feldspathic and semi-pelitic rocks.

Mineral assemblages in semi-pelitic metagreywacke are:

(1) Quartz-plagioclase-muscovite-biotite(-chlorite)

(2) Quartz-plagioclase-biotite-epidote-actinolite

These assemblages belong to the greenschist facies of regional metamorphism, probably the highest-temperature muscovite-biotite

subfacies as defined by Hietanen (1967). The paragenesis of the muscovite-biotite subfacies is illustrated in Figure 4a.

Quartz-feldspathic rocks include feldspathic quartzite, granite, quartz monzonite. Mineral assemblages are more or less similar to those of metagreywacke, but the relative proportions of minerals are quite different. Quartz, plagioclase, and potash feldspar commonly constitute more than 90 percent of the rock. Others include biotite, chlorite, muscovite, epidote, and actinolite. Quartz is pulverized and recrystallized; the bigger relic grains show undulose extinction. Microcline and plagioclase commonly are fractured and rimmed by a mixture of fine-grained pulverized feldspar and recrystallized quartz. Micas are generally aligned parallel to foliation, and are believed to be of metamorphic origin. Epidote occurs as inclusions within plagioclase grains.

II. GARNET-SILLIMANITE ZONE

The rocks in the garnet-sillimanite zone include gneissic quartz monzonite, amphibolite, K-feldspar gneiss, biotite-quartz-feldspar gneiss, quartz-biotite-feldspar gneiss, and mica schist. Except for the quartz monzonite, the protoliths of all other rocks are not completely certain although some local intrusive relationships may indicate that certain rocks, such as some biotite amphibolite,

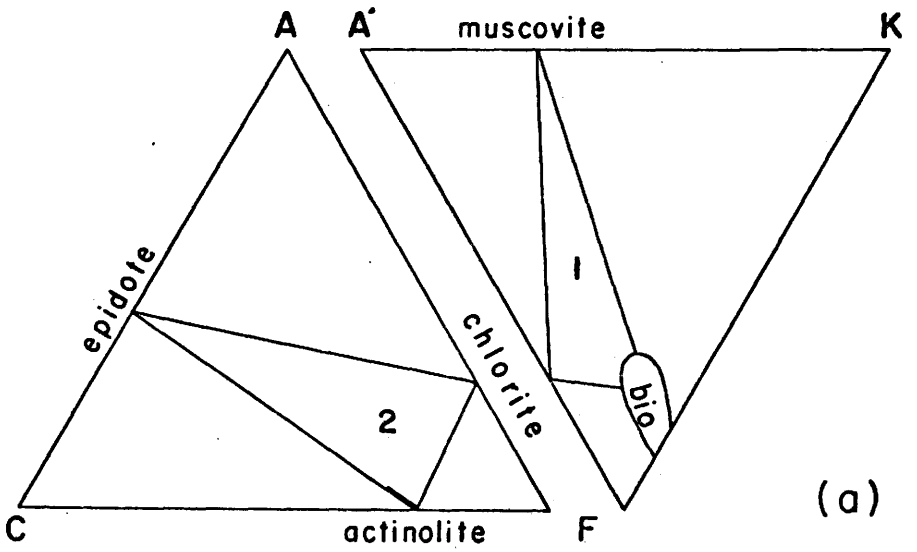
A
A'
muscovite
K
epidote
chlorite
1
2
bio
C
actinolite
F
(a)

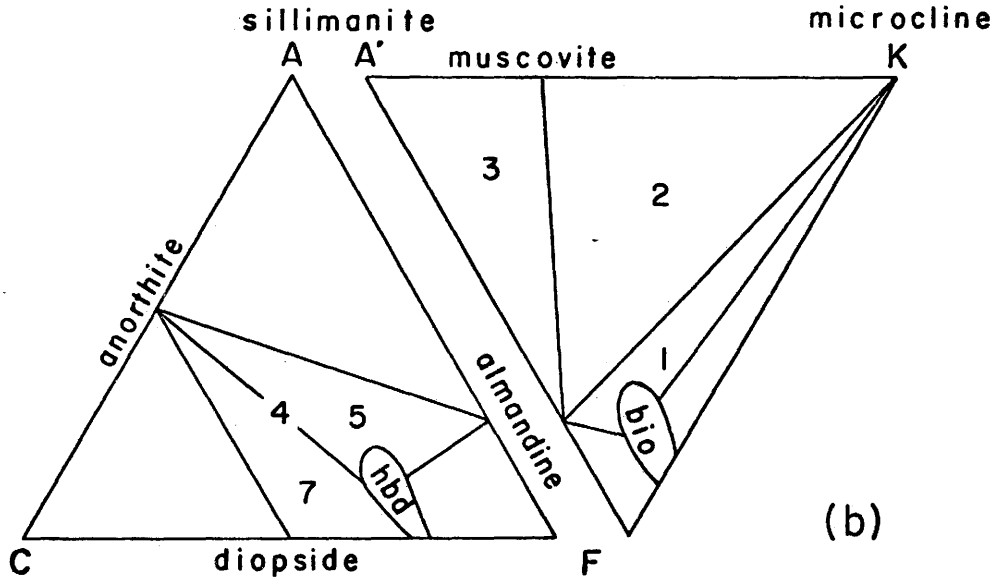
sillimanite
microcline
A
A'
muscovite
K
3
2
anorthite
almandine
1
4
5
bio
hbd
7
C
diopside
F
(b)

are of igneous origin; and gradation of grayish-white gneiss to quartzite may indicate a sedimentary origin.

Mineral assemblages are listed below:

I. Semi-pelitic rocks:

(A) Mica schist:

(1) Quartz-biotite-plagioclase-microcline-garnet

(2) Muscovite-quartz-plagioclase-microcline-garnet

(3) Muscovite-quartz-garnet-sillimanite-plagioclase

II. Basic rocks:

(B) Common amphibolite (biotite less than 5%):

(4) Hornblende-plagioclase(-quartz-biotite)

(5) Hornblende-plagioclase-garnet(-quartz)

(C) Biotite amphibolite (biotite more than 10%):

(6) Hornblende-plagioclase-biotite(-quartz-garnet)

(D) Diopside amphibolite:

(7) Hornblende-plagioclase-diopside

The mineral assemblages are typical of the amphibolite facies of regional metamorphism, belonging to the sillimanite-muscovite subfacies (Hietanen, 1967). The paragenesis of the subfacies is illustrated in Figure 4b. Sillimanite, muscovite, and potash feldspar are associated in some rocks close to the batholith, in which the K-feldspar is regarded as of metasomatic origin.

III. PETROLOGIC INTERPRETATION

In the northwest portion of the batholith in the map area, the biotite zone is assigned to the greenschist facies of regional metamorphism, probably the highest-temperature muscovite-biotite subfacies (Hietanen, 1967). Further northwest, the rocks may belong to the lower-temperature muscovite-chlorite subfacies of the same facies (Henderson, 1967).

The rocks southeast of the sillimanite isograd in the recrystallized area contain mineral assemblages typical of the amphibolite facies. The coexistence of muscovite and sillimanite over a large area suggests that the rocks belong to the sillimanite-muscovite subfacies (Hietanen, 1967).

The regional distribution of diagnostic mineral assemblages indicates that the sillimanite isograd (actually the isograd may lie somewhere further northwest) represent a line of metamorphic break, since sillimanite appears along the isograd very close (i.e. within half a mile or 800 meters) to the rocks containing biotite, epidote, and actinolite. A schematic metamorphic profile across the map area along line A-A' on Figure 3 is made to illustrate the metamorphic discontinuity (Figure 5).

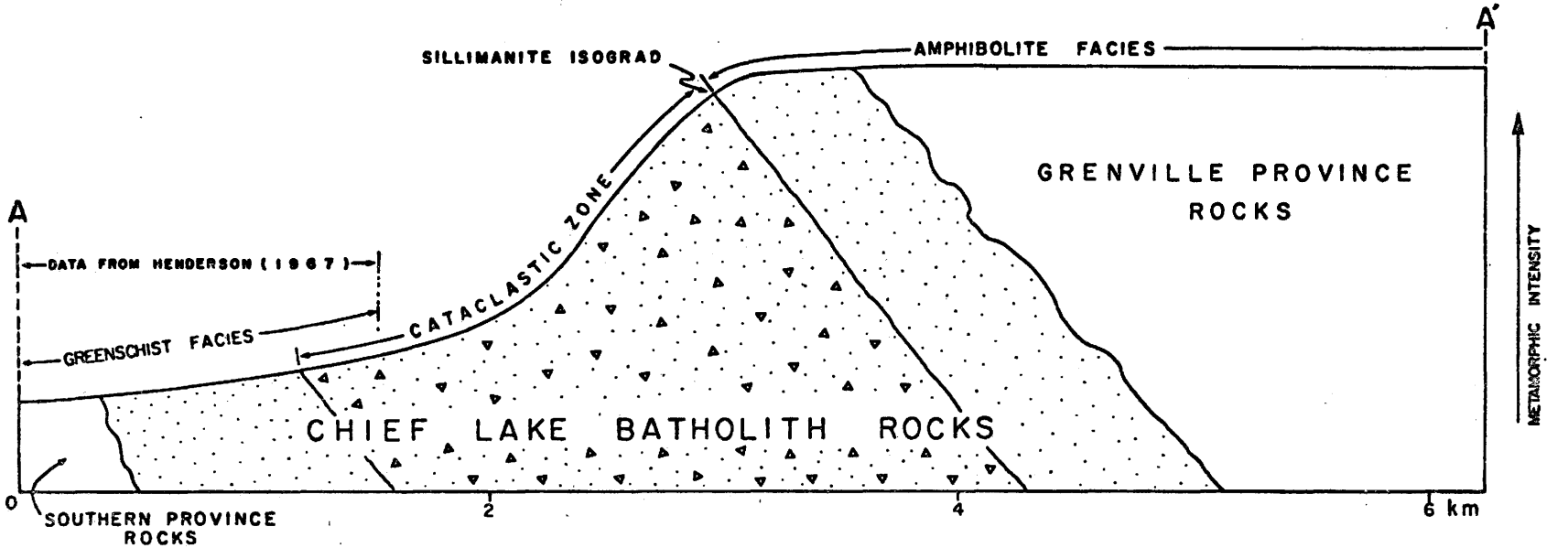

Figure 5. Schematic metamorphic profile along line AA' on Figure 3

The metamorphic gradient rises "gradually" from the lower-temperature subfacies of greenschist facies at the contact between Huronian rocks and batholith (Henderson, 1967) across the northwestern corner of the map area where the rocks belong to the higher-temperature subfacies, then suddenly steepens within half a mile (800 meters) to the sillimanite-muscovite subfacies of amphibolite facies. The proximity of sillimanite-bearing rocks to biotite-epidote-actinolite-bearing rocks indicates that metamorphic gradient is very steep. The metamorphic intensity seems to increase gradually to the southeast of the sillimanite isograd, since the potash feldspar-sillimanite assemblage is found in the semi-pelitic schist in the southeastern border of the area where the muscovite isograd (or the second sillimanite isograd) may be drawn along the border (not shown in the diagrams).

According to Hietanen (1967), the possible P-T conditions for the muscovite-biotite subfacies of greenschist facies are 300° to 350°C and 3,300 to 6,000 bars water pressure; whereas for the sillimanite-muscovite subfacies of amphibolite facies the tentative T-P ranges suggested are 490° to 615°C and 5,000 to 6,700 bars.

CHAPTER 4

STRUCTURAL GEOLOGY

The Chief Lake batholith rocks are characterized structurally by strongly penetrative foliation and mineral lineation. The Grenville province rocks, on the other hand, are characterized by both large-scale and small-scale folds and refolds in gneissic layering. Penetrative foliation transverse to gneissosity surfaces in the high-grade metamorphic rocks was seldom observed. Lineation is conspicuous throughout the whole area, and was found to have been deformed locally by small-scale superimposed folding. An earlier large-scale superimposed fold is truncated by the batholith which has been strongly milled to form the cataclastic zone (Figure 6). These structural data record a serial sequence of tectonic events. The major objective of structural analysis in this research is to describe the deformational history and mechanics of the area by using these data.

I. GENERAL STATEMENT

Fabric Elements and Treatment of Data

Orientations of structural fabric elements recorded in the field include:

(1) Bedding (S_b) of metasedimentary rocks,

(2) Gneissic layering (Sg) of the Grenville province rocks,

(3) Axial trace and axial surface of folds in Sg,

(4) Fold axis,

(5) Foliation (S_f),

(6) Mineral lineation (L_1), and

(7) Fault or shear plane.

The geometric treatment of data for structural analysis has been carried out for both mesoscopic and macroscopic scales. The mesoscopic scale refers to the structure directly observable in a single exposure whereas the macroscopic scale refers to the structure larger than the mesoscopic scale.

All the stereograms of structural fabric elements in the study are made on the lower hemisphere equal-area (Schmidt) projection. Only the diagrams containing more than 80 data points have been contoured. Diagrams are contoured according to the percentage of points per unit area of the net.

Faults

Two faults have been traced in the area. The exposed fault zones contain brecciated rocks, sheared rocks, or quartz-filled stockwork as the one at the small islet in Brodill Lake (Figure 2). These

two faults trend 144 degrees across the lake and either dip steeply to the southwest or are vertical. Towards the east, the faults turn to the northeast, and merge into one fault which could be traced only with difficulty.

Shear Zone

A wide cataclastic zone was mapped in the northwestern portion of the batholith in the map area. The cataclastic zone trends northeast and is about one mile (1.6 kilometers) wide. The southeastern boundary of the cataclastic zone is coincident with the sillimanite isograd, whereas the northwestern boundary lies beyond the map area. According to Henderson's description (1967), the northwestern boundary is a major shear zone along the contact between the batholith and the Huronian metasedimentary rocks.

Within the cataclastic zone, the texture of rocks is blastomylonitic (augen-gneissic) or mylonitic. The milled rocks in the whole area, however, are by no means confined to the cataclastic zone. At many places southeast of the cataclastic zone, rocks with mylonitic texture have been locally recorded, but they are not shown in the geological map.

Structural Subdivisions

The map area is divided into eight structural domains based mainly on apparent structural unity (Figure 6). Excepting domains I and VII, each domain is further divided into subdomains a, b, and so on, on the basis of structural homogeneity. The objective of this kind of detailed division is to facilitate geometrical analysis of structural elements. In general, domain I contains the batholith and migmatitic gneiss in which structural analysis is based on geometries of the penetrative foliation and mineral lineation recorded from meta-igneous rocks; whereas domains II to VIII are all located in the Grenville province and the structural analysis in these domains is based on geometries of gneissosity (instead of foliation), lineation, and folds on both mesoscopic and macroscopic scales. Penetrative foliation is seldom found in the Grenville province rocks, but an early foliation, commonly parallel to the folded gneissosity except in some fold hinges, occurs in the structurally complicated high-grade metamorphic rocks.

II. REGIONAL GEOMETRY

Geometry of Domain I

Domain I comprises the batholith and the migmatitic gneiss in the southwest of the area, and makes up more than one third of the

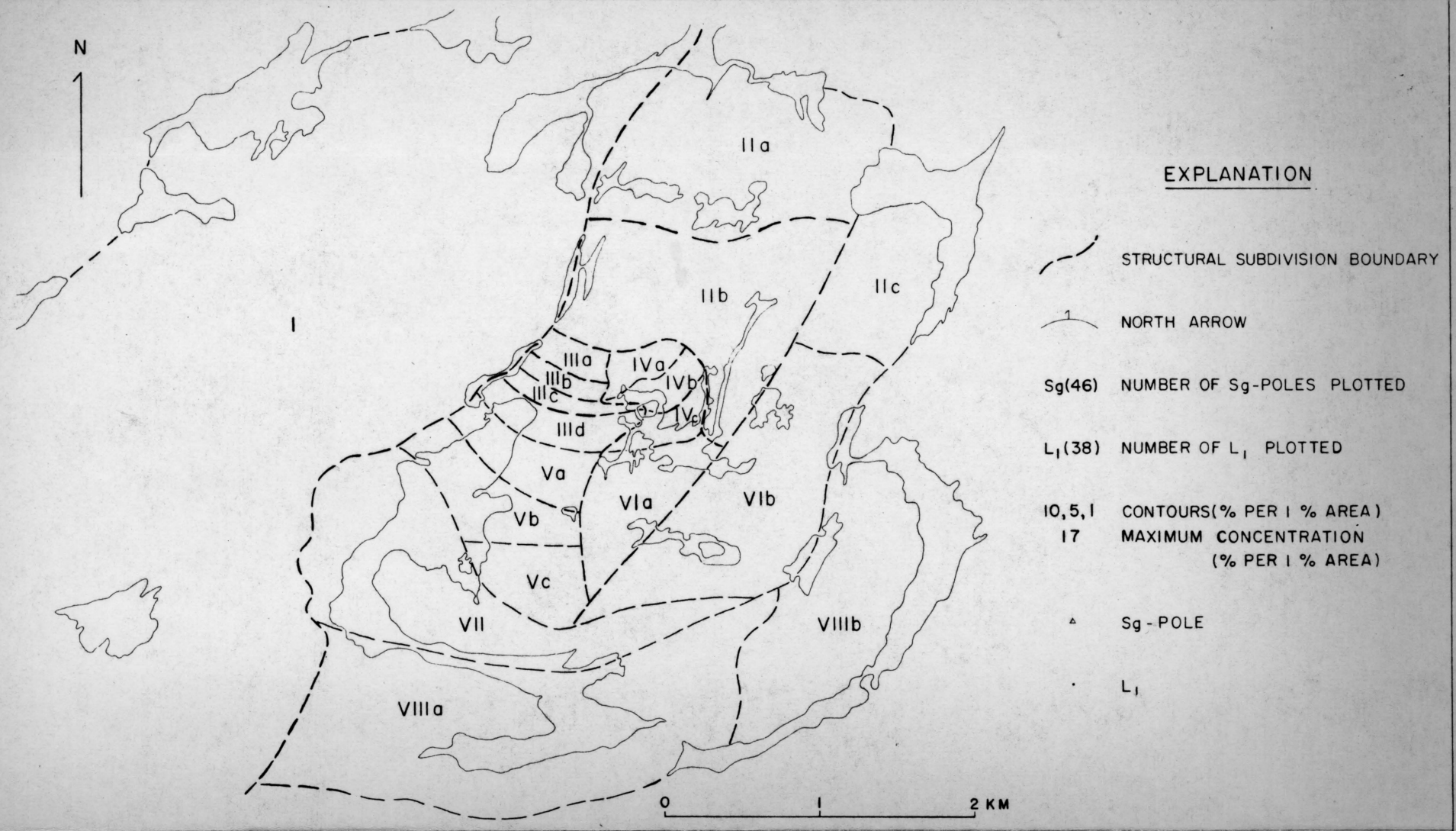

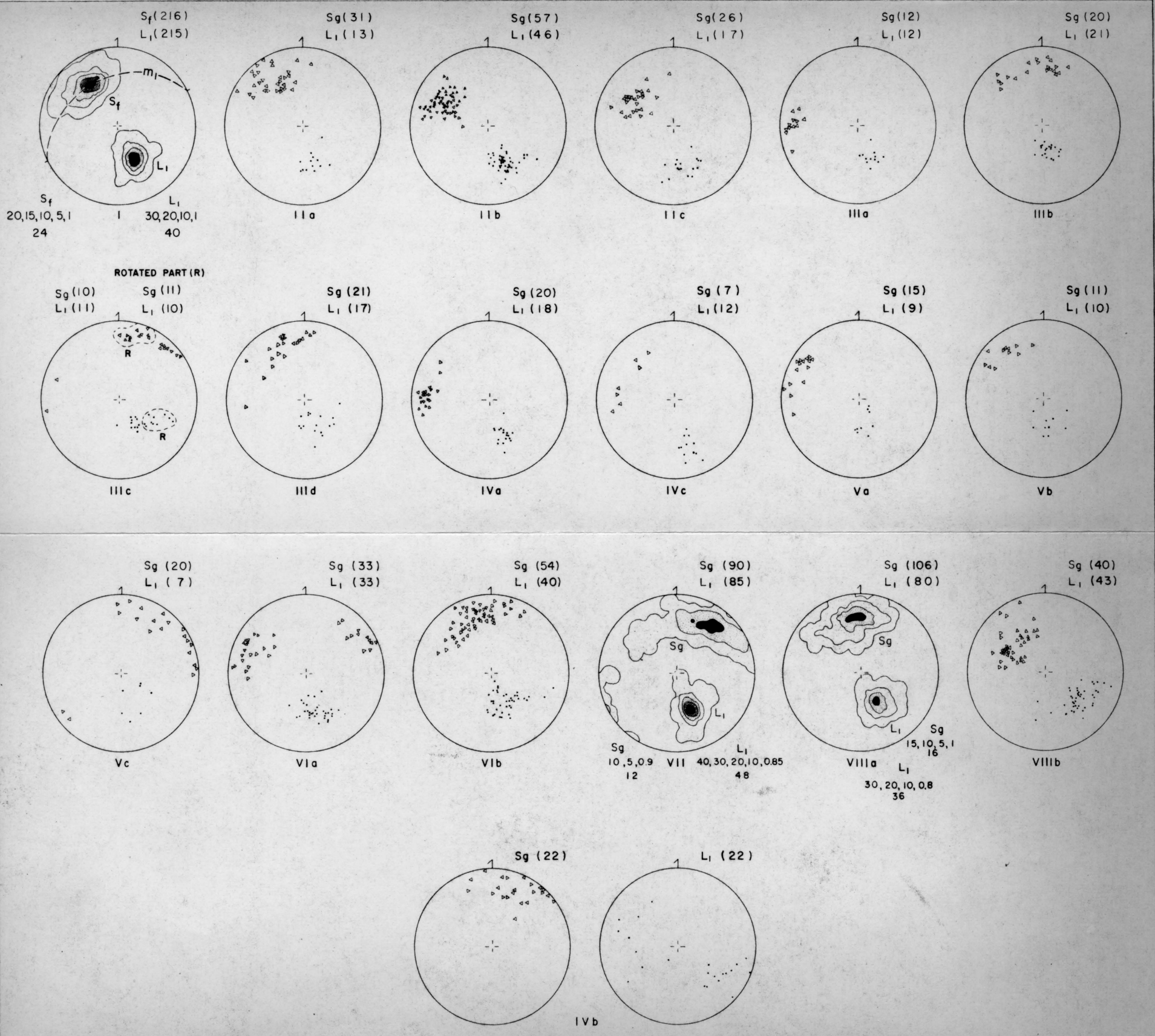

FIGURE 6. STRUCTURAL SUBDIVISIONS AND MACROSCOPIC FABRICS

whole area. The boundary between domain I and other domains is the contact between the batholith and the Grenville province gneissic rocks excepting the migmatitic gneiss (Figure 6).

Domain I is characterized by tectonites containing penetrative foliation (S_f) and mineral lineation (L_1). Mineral lineation and foliation are marked by flattened and elongated quartz and feldspar grains. In general, steeply to moderately dipping foliation and approximately down-dip lineation occur together, but S_f and L_1 may occur separately. In the northwestern portion of domain I (Figure 6), the batholith rocks are within the cataclastic zone and show blastomylonitic texture with microcline porphyroblasts surrounded by a rim of fine-grained plagioclase and microcline mixed with recrystallized quartz. In the southeastern portion of domain I, the rocks are recrystallized and show more blastoporphyritic texture, although local cataclastic texture also can be found. Despite the change in textures of rocks, both foliation and mineral lineation tend to maintain constant orientation over the entire domain.

Numerous foliated and lineated xenoliths occur in the batholith generally with their longer dimensions aligned parallel to S_f.

The macroscopic geometries of S_f and L_1 in domain I are shown on Figure 6. S_f has a dominant east-northeast strike and moderate to steep dip to the southeast; L_1 plunges approximately down the dip of S_f.

The maximum concentration of lineation is 40 percent per one percent area, and plunges 51° at 153° (Figure 6). On the other hand, the poles to S_f show a partial girdle parallel to a great circle centered on the maximum concentration of mineral lineations. The center of the partial girdle of S_f-poles is not identical with the maximum concentration of S_f-poles, so the symmetry of domain I is monoclinic (nearly orthorhombic). The symmetry plane (m_1) is parallel to the partial girdle of S_f-poles (Figure 6).

Geometry of Domains II-VIII

In domains II-VIII, the Grenville province rocks have been folded on both mesoscopic and macroscopic scales, as indicated by the varying gneissosity trends on Figure 7. Despite the complex folding of gneissic layering, the mineral lineations maintain the same orientation, that is, plunging to the south-southeast at angles of about 50°-60°. Exceptions occur locally, especially in the hinge zones of macroscopic folds, where type 3 mesoscopic folds (discussed later) are developed with deformed lineations around their hinges. In dis-

cussing regional geometries, the deformed lineations recorded from comparatively small and restricted areas (such as hinge zones of macroscopic folds) are ignored in the geometric analysis.

In order to discuss the regional fold geometry, the macroscopic folds in the map area from northwest to southeast are designated as fold 1, fold 2, ..., and so on (Figure 18).

Domain II comprises the northeastern part of the map area, where the gneissosity of the rocks generally strikes northeast and dips moderately to the southeast (Figure 6). The parallelism of the gneissosity over the whole domain suggests that the rocks were not involved in macroscopic folding within the domain, and distinguishes domain II from the domains to the south.

Domains III and IV comprise the area of prominent macroscopic refolding; an amphibolite marker in the middle of the refolded area is used to separate the two domains. Subdomain IIIa lies on the north limb of fold 1, while subdomain IIIb comprises rocks on the south limb of fold 1 or the western part of the north limb of fold 2 (Figures 6 and 18). Subdomains IIIc and IIId occupy the western part of the north and the south limbs of fold 3, respectively. Subdomains IVb and IVc lie on the eastern part of the north and south limbs of fold 3, respectively.

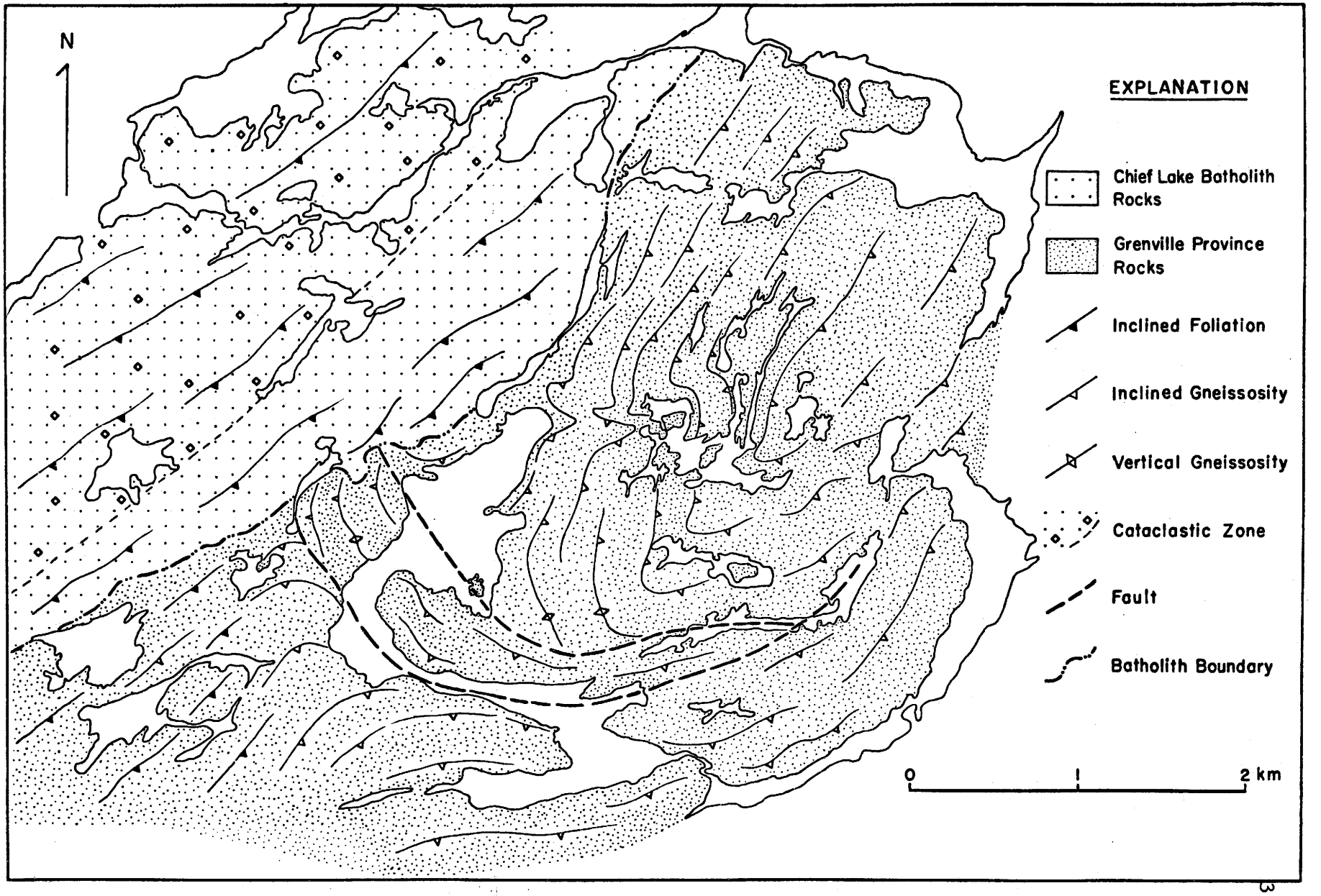

Figure 7. Trend of Foliation and Gneissosity

Domains V and VIII comprise the outer zones of the northwest and southeast limbs of fold 5, respectively. Domain VI constitutes the core of fold 5. Finally, domain VII lies between two faults in the map area and also comprises the nearby rocks apparently affected by faulting.

The macroscopic geometries of Sg and L_1 in each of domains II-VIII are shown on Figure 6. Petrofabric diagrams of mineral lineation show that, in most places except domain IVb, the penetrative lineation is consistently oriented in the same general orientation.

Subdomain IVb comprises several small folds of type 3 (discussed later) and the lineation in the subdomain is curved. Therefore, the data of subdomain IVb are excluded in the general analysis of regional geometry. The macroscopic geometries of total S_g and L_1 in the Grenville province rocks (excluding subdomain IVb) are plotted on Figure 8a. On this figure, the geometric fabric shows an orthorhombic symmetry. One symmetry plane (m_1) is normal to the maximum concentration of lineation. The other symmetry planes intersect in the maximum concentration of mineral lineation; one (m_2) passes through the center of Sg-pole girdle, and the other (m_3) is normal to the Sg-pole center.

Figure 8

(a) Orthorhombic symmetry of 539 S_g-poles (contours - 5%, 3%, and 1% per 1% area) and 468 L_1 (contours - 20%, 15%, 10%, 5%, and 1% per 1% area) in domains II-VIII excluding subdomain IVb. m_1, m_2, and m_3 are symmetry planes.

(b) Coincidence of the S_g-pole center and S_f-pole maximum concentration, as well as parallelism of the mineral lineations in domain I (L_1^f) and domains II-VIII (L_1^g).

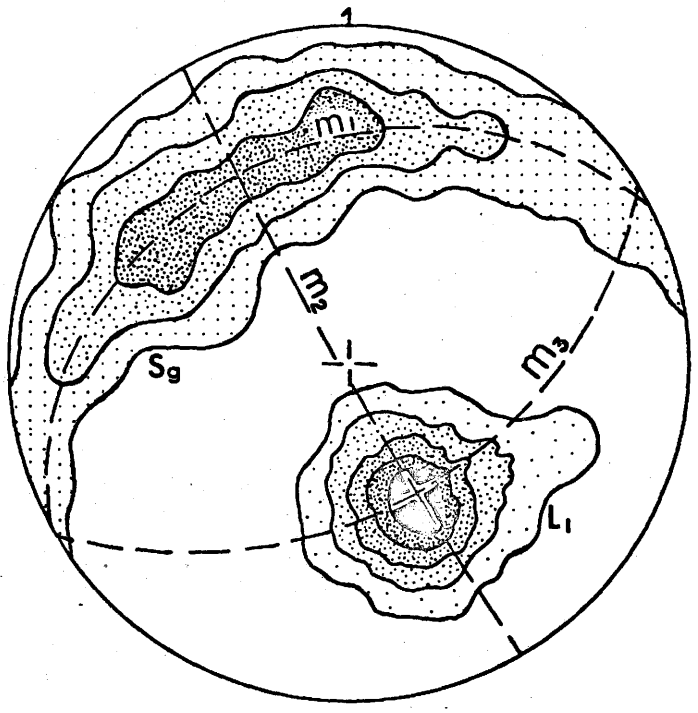

a

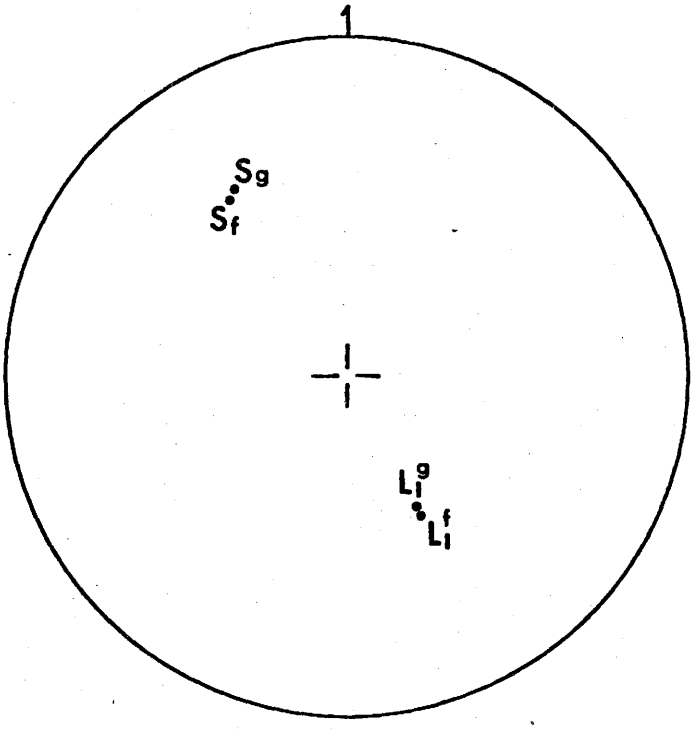

b

Summary of Regional Geometry

Domain I comprises the portion of the area in which mineral lineation and foliation constitute the dominant penetrative structures, whereas domains II-VIII are in the Grenville province, where gneissosity is much more prominent than foliation and most mineral lineations show consistent orientation.

Since the center of Sg-pole girdle of the Grenville province rocks is so close to the maximum concentration of S_f-poles of the batholith, and the maximum concentrations of mineral lineation of the two portions are almost identical (figure 8b), the symmetry plane (m_1) is common for S_f and S_g in the whole area studied, and is found to be normal to the penetrative mineral lineation.

In the cataclastic zone, the mineral lineation developed on the shear plane parallels all the penetrative linear structures in the map area. This may imply that the cataclasis was concurrent with the regional development of mineral lineation as well as all other linear structures further southeast.

III. GEOMETRY OF MESOSCOPIC FOLDS

Four different types of mesoscopic folds were found in the map area: type 1 is a similar fold with penetrative mineral lineation parallel to the fold axis; type 2 is a similar dome-like fold with

penetrative mineral lineation; type 3 is also a similar fold but with deformed mineral lineation on the folded gneissosity surface (Figure 9); type 4 is a combined similar and concentric fold with deformed mineral lineation around its hinge. Folds of type 1 include not only mesoscopic but also macroscopic folds, while folds of the other types are found only on the mesoscopic scale.

Type 1 Folds

Mesoscopic folds of type 1 generally are similar folds. The strikes of the axial surfaces of these folds do not vary over a small area (e.g., a hand specimen or a small exposure); however, on a larger scale type 1 folds are asymmetrical, non-planar cylindrical folds.

In most cases, the axial surfaces of type 1 folds do not parallel the penetrative foliation but fold axes are all parallel to the penetrative mineral lineation (Figure 9a). This kind of fold was found not only in the Grenville province but also in the quartzite xenoliths in the batholith. An example of these folds is given in Figure 10 (see below). The localities as well as the fold axes and the poles to axial planes (only for small outcrops) of type 1 folds are shown in Figure 11.

Figure 9

Sketch of different types of fold. L_1, mineral lineation.

(a) Type 1 fold. Axial surface can be in any orientation as long as it contains the fold axis parallel to the regional mineral lineations.

(b) Type 2 fold. Mineral lineations parallel the elongation of the fold body and penetrate the folded gneissosity.

(c) Type 3 fold. Deformed mineral lineations lie on a plane (shaded). AP, axial plane. a, flow direction. Fold axis is not parallel to the regional mineral lineations which subparallel the a-direction.

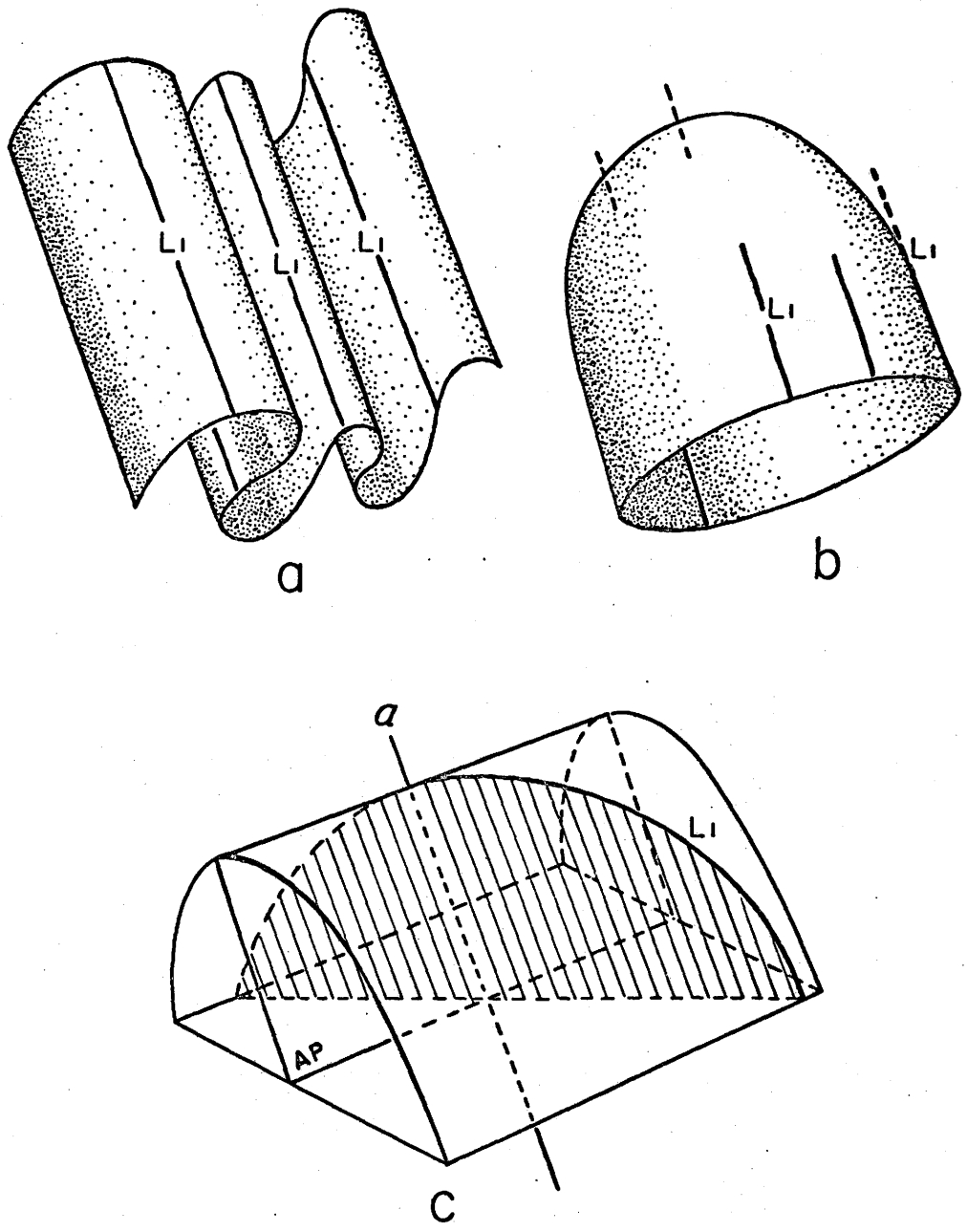
L1
L1
L1
a
L1
L1
b
a
L1
AP
c

Figure 10

Projection of fold 9 as an example of type 1 folds. Attitudes of gneissic layerings are plotted as great circles which intersect at a common point β. All mineral lineations (L_1) parallel the β-axis. AS, axial surface. m, symmetry plane.

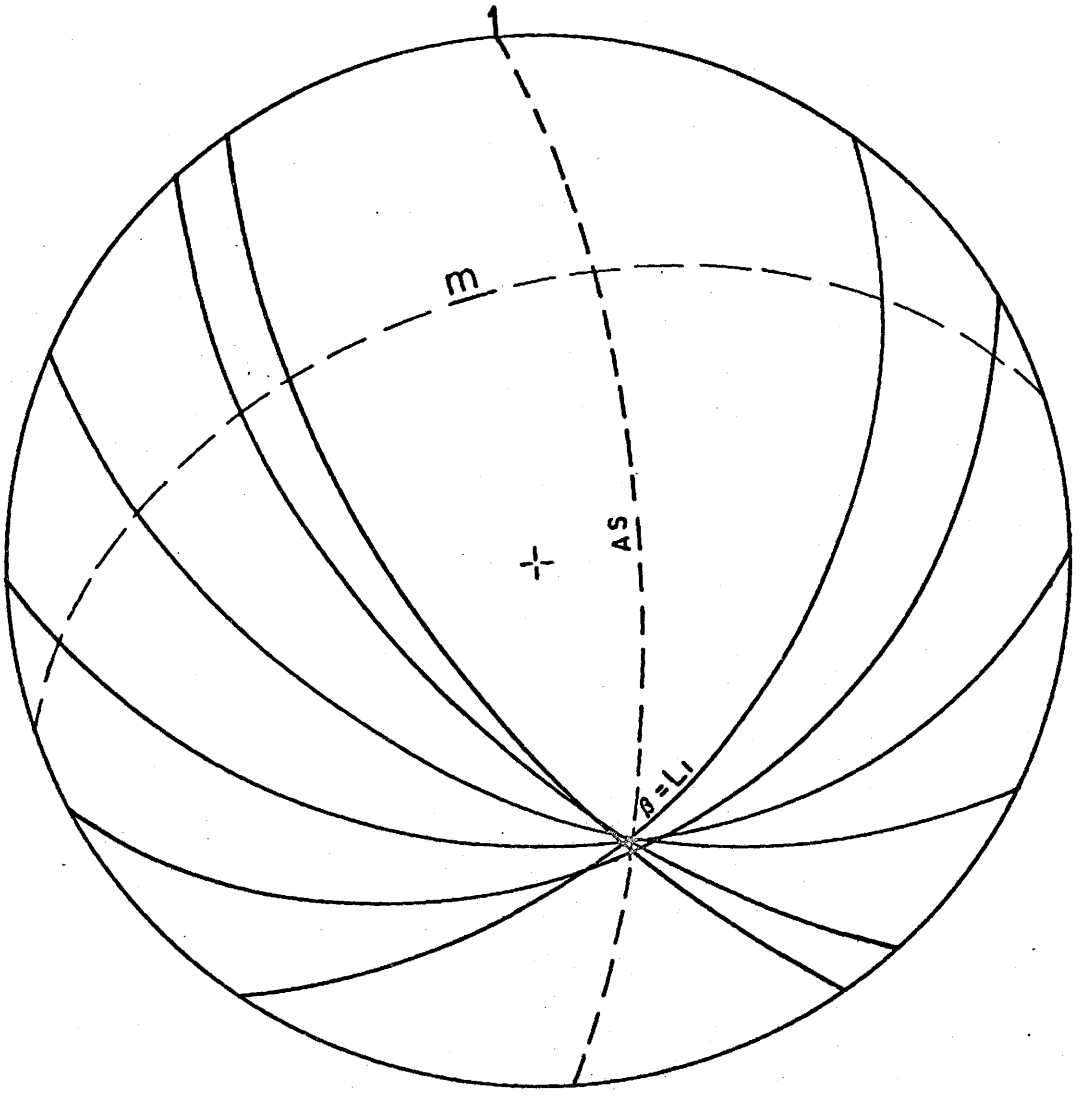
1
m
AS
β=Li

Figure 11

Fabric symmetry of axial surfaces and fold axes of type 1 mesoscopic folds. Diamonds, localities of folds (solid, antiform; open, synform; half solid, reclined fold); small triangles, poles of axial surfaces; dots, fold axes. Note that mineral lineations are parallel to the fold axis in each fold.

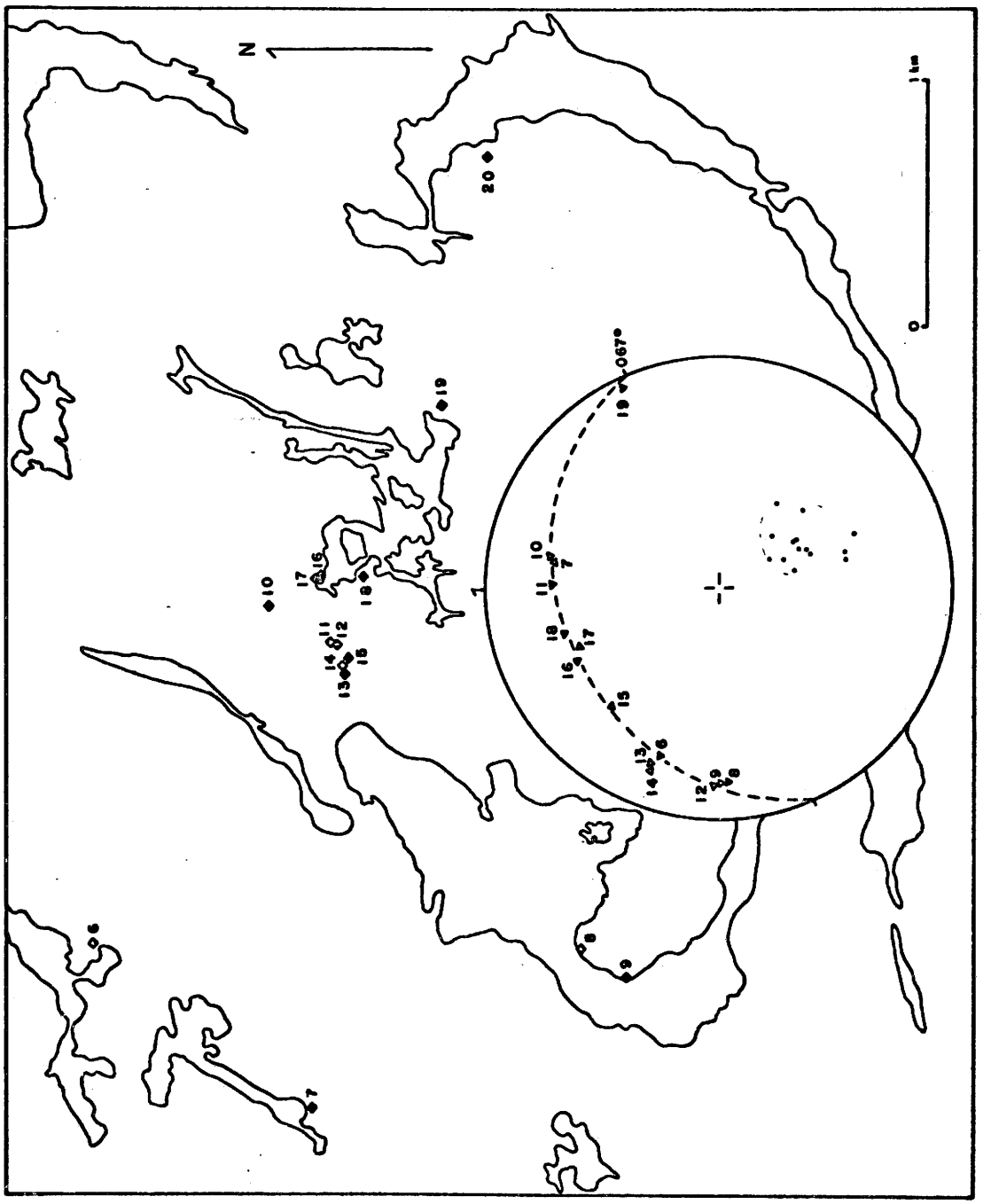
N
1 km
0
067°

In Figure 10, the dip and strike data of the folded gneissosity of fold 9 (Figure 11) are plotted as great circles on the stereogram. The great circles intersect in a common point, β, which is referred to as the β-axis. The mineral lineations on the gneissic layering all parallel the β-axis, i.e. β=b=B as defined by Wilson (1967); B-axis is referred to as the hinge line while the b-axis of a cylindrical fold is defined as the direction of any straight line (such as L_1 in type 1 fold) that can be drawn on a curved bedding plane within the fold in question.

On the inset projection of Figure 11, the poles to axial surfaces of the type 1 folds in the map area lie on a great-circle girdle centered on the common fold axis which is parallel to the penetrative mineral lineation developed on the folded gneissosity. Many such non-planar cylindrical folds have been treated as products of coaxial repeated folding: a planar cylindrical system is superimposed upon a non-planar (initially planar) cylindrical system with the two generations of fold axes in common (Clifford, et al., 1957; Turner and Weiss, 1963). However, this interpretation of coaxial refolding may not be correct in the case as found in the map area. It will be shown later that all the axes of the inherited folds would be rotated into parallelism with one another during a later strong deformation. Thus, the fold axis of a second generation fold was

not necessarily parallel to that of the first generation before being subjected to the later rotation during strong deformation.

Type 2 Folds

Folds of type 2 are "eyed" folds which are generally symmetrical, similar, non-planar, but conical. Most of the closed folds show an elongated elliptical cross-section on the erosion surface (Plate 3). Mineral lineations (L_1) developed on the closed gneissic layering are parallel to one another.

The axial plane containing the long axis of the elliptical outcrop is parallel to the dominant attitude of the surrounding gneissic layerings (Plate 3). If the pole of this axial plane is plotted on Figure 11, it will also lie on the great-circle girdle containing the poles to the axial surfaces of type 1 folds.

By using the data obtained from field observation, a sketch diagram of the dome-like fold is shown in Figure 9b. In the diagram, one can see that first, the gneissic layering is closed at the section normal to the elongation of the fold; second, all the mineral lineations are parallel to one another; and third, the mineral lineations parallel the elongation of the fold body and penetrate the folded gneissosity.

Plate 3

"Eyed" folds (type 2 folds). (a) in domain VII

(b) in subdomain VIb.

(a)

(b)

The "eyed" fold could result from one of the following processes: (1) a previous fold, either similar or concentric, subjected to a later buckling with a component of compression parallel or subparallel to the first fold axis; (2) a previous fold, either similar or concentric, subjected to a heterogeneous simple shear which is normal or subnormal to the first fold axis (otherwise, the first fold axis would be rotated to parallel the shear direction); (3) an initial plane subjected to a heterogeneous simple shear normal or subnormal to the plane. The first two processes are superimposed foldings while the third one is a single conical flow-folding. It is not certain when the folding and/or refolding took place and also not certain which process it has undergone, since the fold could develop either before or during an early stage of the final strong deformation.

The pattern of type 2 folds might have been dome-like originally but modified further by later homogeneous strain. This modification would not fundamentally affect the type of closed form and thus the cross-sections of the dome-like folds would be elongated elliptical.

Type 3 folds

Folds of type 3 generally are cylindrical, planar, similar folds. They are found only in the Grenville province rocks and are only of mesoscopic scale. These folds occur mostly in the hinge zones of macroscopic folds (belonging to type 1 folds).

The limbs of type 3 folds generally are asymmetrically inclined with respect to the axial plane. The axial planes are more or less parallel to the penetrative foliation. Mineral lineations developed on the folded gneissic layering are curved (Plate 4). It is obvious that folds of type 3 were formed in rocks which had been previously metamorphosed and lineated. Since the locus of the deformed mineral lineation lies on a plane, most of type 3 folds belong to similar slip folds formed by inhomogeneous simple shear (Turner and Weiss, 1963; Ramsay, 1967). The slip direction (a), also known as the flow direction, corresponds to the intersection line of the axial plane and the locus of early lineations lying on a plane, and is also designated as the a kinematic axis. The b kinematic axis, on the other hand, refers to the line normal to a but lying on the axial plane.

Plate 4

Deformed mineral lineations on Sg in type 3 folds.

(a) Fold 28 in subdomain IVa.

(b) A type 3 fold developed on the hinge of macroscopic fold 5, boundary between subdomains VIa and VIb.

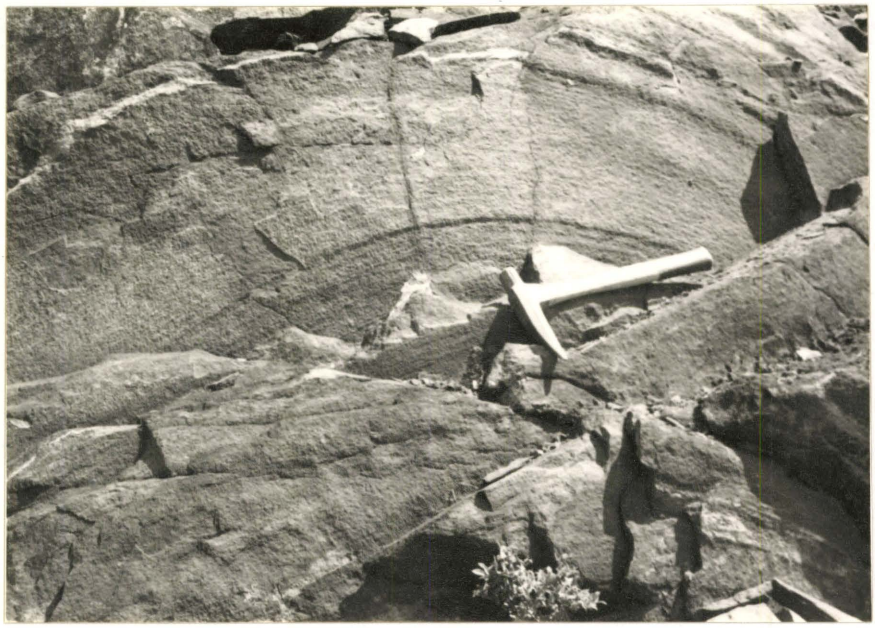

(a)

(b)

Ten folds of type 3 have been analysed; of these, seven are in the northeastern portion of the map area and three are from the hinge zones of macroscopic folds. Fold 25 is presented in Figure 12 to demonstrate the symmetry of this type of fold in which the fold axis is inclined to both kinematic axes a and b. Since the fold axis (β) is not the kinematic axis b, the plane of symmetry (m') of the movement picture is inclined to that of the fold (m); the former plane (m') also is not coincident with the lineation locus as shown in Figure 12. The lineation locus lies on a plane and thus the fold belongs to a perfect similar-fold model. Nine of the ten mesoscopic folds of type 3 analysed show that an inhomogeneous simple shear was responsible for the folding; only fold 22 is an exception.

Analysis of fold 22 by rotating the axial plane to the vertical position and the fold axis to the horizontal shows that the fold may contain a slight buckling component of the imperfect similar type (Figure 13). After rotation, the southeastern segment of the locus of mineral lineation appears to lie on a great circle whereas the northwestern segment seems to lie on a small circle, although all this is not definite because the lineation locus is almost normal to the fold axis (β), i.e. there is not much difference between a small circle and a great circle in this orientation. Nevertheless, the slightly-distorted

Figure 12

Projection of fold 25 as an example of type 3 folds. Attitudes of gneissic layerings are plotted as great circles which intersect at a common point β. Deformed mineral lineations (L_1) lie on a plane which intersects the axial plane (AP) in a direction a oblique to the intersection of Sg and axial plane. m and m' are the symmetry planes of the fold and the movement picture, respectively.

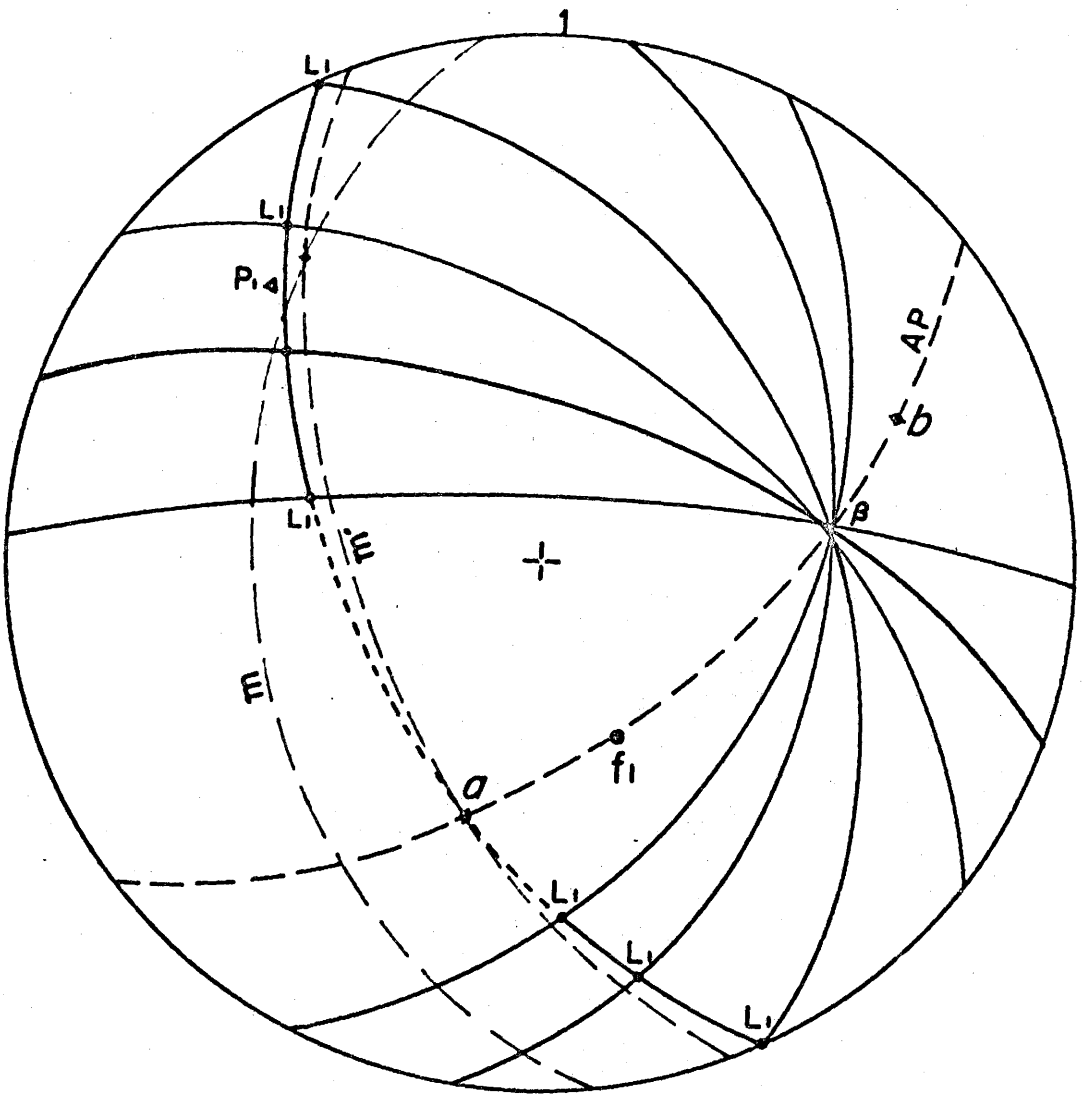
1
L1
L1
P1
L1
E
E
a
f1
L1
L1
L1
AP
b
β

Figure 13

Analysis of fold 22 by rotating the axial plane to the vertical position and the fold axis to the horizontal.

(a) Before rotation. Passive Sg contains passive L_1. Axial plane (broken line of great circle) contains β-axis.

(b) After rotation. L_1 locus shows partly great circle and partly small circle.

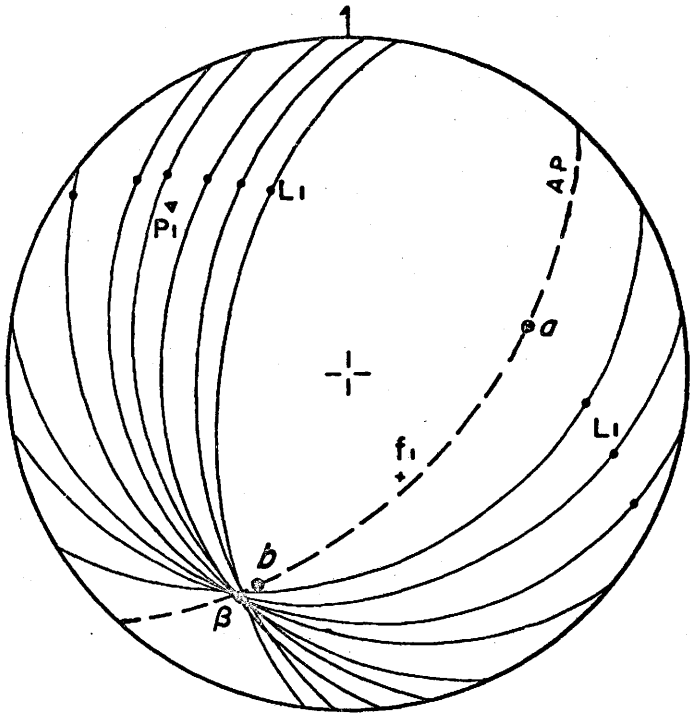

a

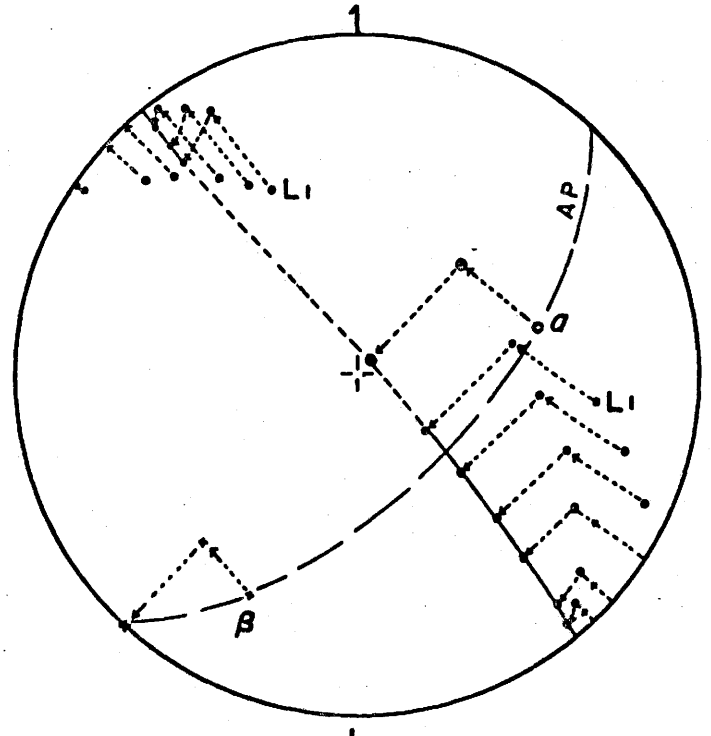

b

lineation locus appears to have been formed by buckling (flexural-slip mechanism) followed by simple shear (Ramsay, 1967, pp. 483-484).

Figure 14 shows the projections of a directions, fold axes, and poles to axial planes of type 3 folds in the map area. It is interesting to note the following fabric geometries: (1) The axial planes of the folds show a fairly constant orientation, indicating that the orientations of the fold-forming translation (Ramsay, 1967, p. 471) were fairly constant over the area studied. (2) Folds 28-30 were measured in the hinge zones of macroscopic folds. The structural data of these three folds, including a directions, fold axes, and axial planes are systematically rotated at a certain angle with respect to the rest of folds, suggesting that the three folds perhaps were subjected to a later rotation after deformation of the mineral lineations. (3) The a directions show comparatively slight changes in orientation through the apparently non-rotated area. In contrast to this, fold axes are more variable, either because the surfaces on which the folds were developed were themselves variably oriented, or because the amount of compressive strain accompanying the folding was variable during the deformation, or a combination of above-mentioned factors (Ramsay, 1967).

Figure 14

Projections of $\underline{a}$ directions, fold axes, and poles to axial planes of type 3 folds.

Solid diamonds (antiforms) and open diamonds (synforms), localities of folds; solid dots, $\underline{a}$ directions; crosses, fold axes; open triangles, axial-plane-poles of type 3 folds; solid triangle, axial-plane-pole of macroscopic fold 5.

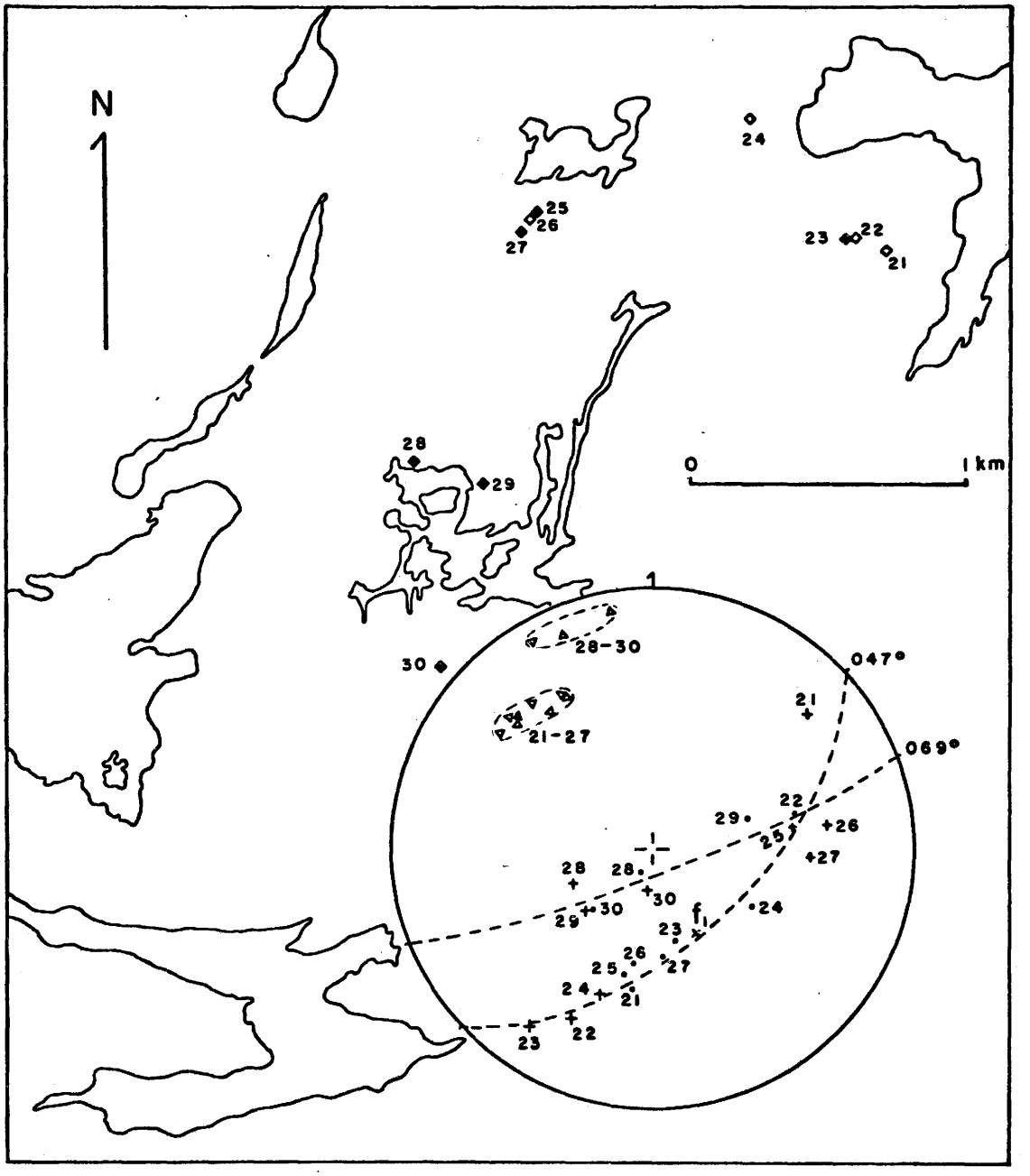
N
24
25
26
27
23
22
21
28
29
0
1 km
1
30
28-30
047°
21
21-27
069°
22
29
25
+26
+27
28
28
30
30
29
+30
24
23
26
25
27
24
21
23
22

It will be shown later that among the five macroscopic folds, which have parallel axes plunging moderately to steeply to the south-southeast, the axial trace of fold 5 is the least curved and is almost a straight line subparallel to the regional gneissosity in the apparently non-folded area (Figure 18). Therefore, it is here assumed that fold 5 represents the original attitude of the first-generation macroscopic folds in the map area. The orientation of the fold axis and the pole to the axial surface of fold 5 are plotted in Figures 12 and 14 as f_1 and P_1, respectively. If the angle between the second b kinematic axis and the first fold axis (f_1) is designated α and the angle between the flow direction (a) of the superimposed movement and the pole (P_1) to the axial surface of first fold is designated β, then one pair of angles α and β can be computed from each fold of type 3. The relation of these angles can be used to determine the nature of the interference patterns in superimposed folds (Ramsay, 1967, pp. 518-533).

Figure 15 shows the angles α and β of the small superimposed folds (type 3) in the map area, assuming the attitude of fold 5 represents that of the first-generation fold. Because folds 28-30 might have been rotated after deformation of mineral lineation as noted before, and also because these three folds developed in the macroscopically refolded area, the attitude of fold 5 is thus not valid for comparison with them. Consequently, the β-angles of folds 28-30 are relatively smaller than those of

Figure 15

Angles α and β of superimposed folds (type 3).

Numbers show different folds; their localities are shown in Figure 14. Letters A-I represent the different interference patterns defined by Ramsay (1967, Figure 10-13, p. 531).

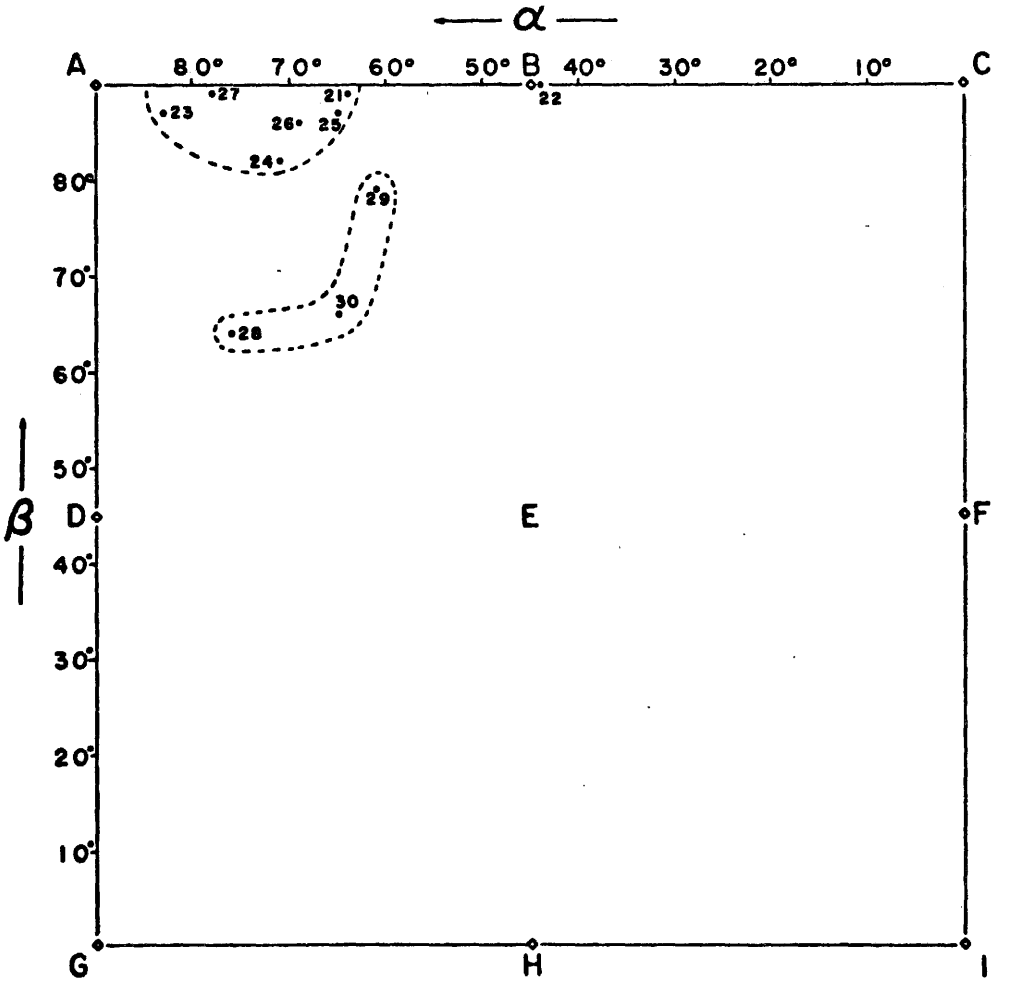
α
A
8.0°
7.0°
6.0°
5.0°
B
4.0°
3.0°
2.0°
1.0°
C
27
21
23
26
25
22
24
80°
29
70°
30
28
60°
50°
β
D
E
F
40°
30°
20°
10°
G
H
I

the other folds. However, the α-angles of these three folds are similar to those of the others, indicating the refolding or rotation did not change the orientation of the first fold axis. On the other hand, in the apparently non-folded area, only fold 22 is isolated from the others; its α-angle is only 44 degrees, probably because the fold was initiated by buckling instability within the competent layer and then modified by the process of flattening and shear parallel to the axial surface (Figure 13). The rest of the type 3 folds, including folds 21 and 23-27, are all typically similar folds formed by inhomogeneous simple shear with shear axes constantly oriented. Their mineral lineation loci all lie on planes. The angles α and β of these six folds show a fairly constant relation between the two generations of folds (Figure 15). Angle α is within the range from 64° to 83° whereas angle β is between 82° and 90°. In other words, the flow direction of the superimposed movement is nearly lying on the axial plane of the first folds. According to Ramsay (1967, p. 531), the interference patterns in this case should be a dome-like structure. Unfortunately, no such structures with deformed mineral lineations were ever observed in the map area.

Reviewing the six "normal" folds (21 and 23-27) in Figure 14, one can see that (1) the axial planes of the superimposed folds

(type 3) are more or less parallel to that of fold 5 and the regional penetrative foliation (Figure 7); (2) the great-circle girdle containing fold axes as well as $\underline{a}$ directions of the mesoscopically-superimposed folds (type 3) also contains the axis (f_1) of fold 5 - the major fold in the map area; (3) all $\underline{a}$ directions are fairly close to f_1 which is parallel to the regional mineral lineations and the axes of all other macroscopic folds and all refolds (shown later), indicating the shear (flow) direction of the superimposed movement was nearly the same as the flow direction of all passive previous fold axes.

Type 4 Fold

Fold of type 4 is a combined similar and flexural-slip fold with deformed mineral lineations on the limbs. A type 4 fold was found only at one outcrop - fold 20 (Figure 11) - on the eastern border of the map area.

The mineral lineation observed in the field is marked by elongated feldspar and hornblende grains developed within the folded layered amphibolite. The lineation is curved and can be traced around the hinge of the fold, of which the fold axis is assigned to $B=\beta$. The angle $L_1 \wedge \beta$ is variable, so it is certain that similar folding is in part responsible for the deformation. However, when these deformed lineations are plotted on a stereogram (Figure 16a), their locus appears

like a small circle rather than a great circle. Obviously, there seems to be an additional rotation about the fold axis caused by a later, co-axial, flexural-slip buckling, which carried the points (poles of mineral lineation) off the great circle to form a small-circle-like locus. The distortion of the lineation is more easily recognized in Figures 16b and 16c, in which the axial plane is first rotated to a vertical position, and second, the fold axis, β, is moved to the horizontal position. The mineral lineations then show two separated segments of neither great-circle nor small-circle locus. Since the lineation locus is asymmetric and discontinuous, the a direction of the relatively-earlier shear mechanism can not be defined.

It is interesting to find how the pattern of the corresponding Sg changes when the deformed lineations are "straightened". Lineation of measurement No. 5 in Figure 16(c) is horizontal and is assumed to be the only one non-deformed linear structure in the fold during the combined similar and concentric folding. The angle between the lineation No. 5 and the fold axis (β) is the so-called "original angle" (Ramsay, 1967) which is 47 degrees in this fold. If all the other directions of lineation in Figure 16(c) are restored to parallel lineation No. 5 which is horizontal and oriented at 135 degrees (Figure 16d), then the corresponding Sg are rotated to form a fold whose axis is

Figure 16

Analysis of fold 20.

(a) Passive Sg containing passive L_1 (solid dots) are plotted as great circles which intersect at a common point β. Broken great circle (AP) is axial plane. Numbers are measurement numbers.

(b) Axial plane is rotated to the vertical position and the fold axis (cross) is moved to the horizontal. Solid triangles are Sg-poles.

(c) The L_1 locus shows two separated segments of neither great circle nor small circle.

(d) The deformed L_1 are "straightened" to parallel lineation No. 5, and the corresponding Sg-poles are rotated to form a fold whose axis is oriented parallel to the "straightened" lineations.

(e) Lineation No. 5 is moved back to its present position (diagram a) via the same path it was rotated to the horizontal, the Sg-poles are rearranged to show the original fold form before the last deformation.

(f) Fold axis of (e) is moved to plunge 56^{o} at 152^{o}, and the axial-plane-pole (open triangle) is rotated to lie on the great-circle girdle containing the axial-surface-poles of all type 1 folds (Figure 11).

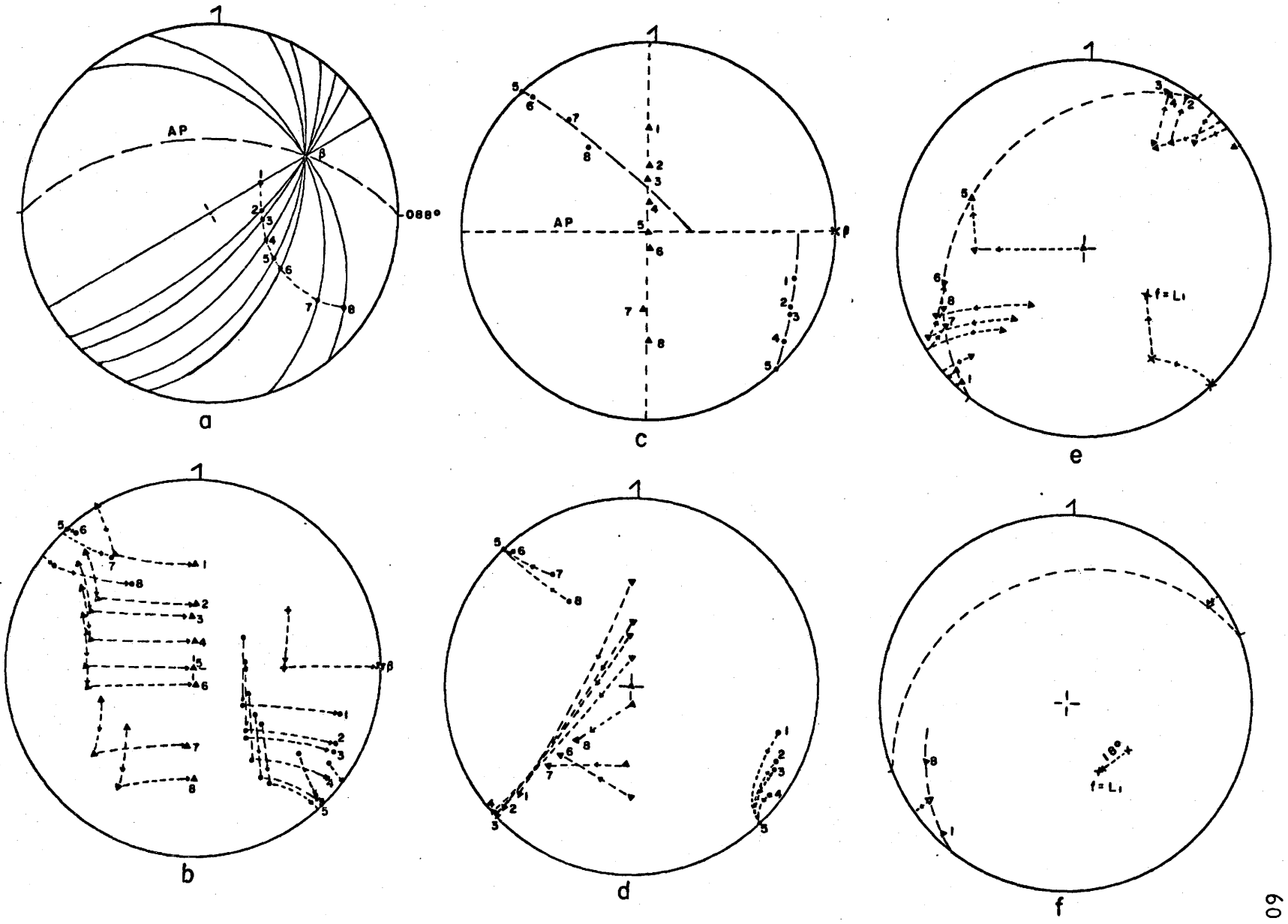
1
AP
β
088°
1
2
3
4
5
6
7
8
a
1
5
6
7
8
AP
β
1
2
3
4
5
6
7
8
1
2
3
4
5
c
1
3
2
5
6
8
7
1
f = L1
e
1
5
6
7
8
1
2
3
4
5
6
7
8
β
1
2
3
4
5
6
7
8
b
1
5
6
7
8
1
2
3
4
5
6
7
8
1
2
3
d
1
8
18°
f = L1
1
f

oriented parallel to the "straightened" lineation, i.e. a fold of type 1. When lineation No. 5 is moved back to its present position (Figure 16a) via the same path it was rotated to horizontal, the Sg-poles are re-arranged to show the pattern of the original fold before the last deformation. In Figure 16(e), the original fold is obtained, in which all lineations are parallel to the fold axis plunging 55° at 125°.

Reviewing the petrofabric diagrams in Figure 6, one can see that the mineral lineation of subdomain VIIIb is relatively rotated from south-southeast to southeast as compared to those in the neighbouring subdomains VIb and VIIIa. The dominant trend of lineations in subdomain VIb plunges 56° at 154° while that of subdomain VIIIa plunges 56° at 150°. Therefore, it is assumed that the "normal" lineation in subdomain VIIIb before rotation plunges 56° in the 152°-direction. If the fold axis in Figure 16(f) is rotated to parallel the regional "normal" lineation, then the pole (open triangle) of the axial plane, which is assumed at the middle point between Sg-poles 1 and 8 (measured at the inflexion points of limbs) in Figure 16(f), will move to a new position plunging 10° at 048°. The new position of the fold axis in Figure 16(f) falls in the fold axes area in Figure 11 while that of the pole to the axial plane lies on the great-circle girdle containing the poles to the axial planes of all type 1 folds in the map area. Hence, it is proved that before the later rotation and folding, fold 20 was one of the folds of type 1.

Parasitic Folds

In general, all the S- and Z-folds in the map area belong to type 1 folds discussed above, and appear to have resulted from the macroscopic folding of the first generation (Figure 17). The macroscopic folds of the second generation might have their own congruous minor (or parasitic) folds, but none of them was ever observed; nor was any real combined superimposed minor-fold pattern found in the field. Although Plate 5(b) taken in subdomain IIb shows a small interference pattern of S-fold superimposed on Z-fold, it is probably a local disharmonic case.

A small gentle fold of macroscopic scale, whose axis extends only about 300 meters between fold 4 and fold 5, is not named. The limbs of the fold were slightly wrapped, yet the folding seems to have been responsible for the development of the local small Z-folds (Plate 5a) on its north limb, which obviously are not compatible with the surrounding S-folds on the northwest limb of fold 5 (Figure 17).

Not less than seven minor Z-folds were observed in domain VII, which are not congruous with the northwest limb of fold 5 (Figure 17), providing a clue to support the conclusion that domain VII was probably shifted westwards (between the two faults across Brodill Lake) from the southeast limb of fold 5 to its present position.

Plate 5

Parasitic folds.

(a) Z-fold on the northwestern part of subdomain VIa.

(b) S-fold in subdomain IIb. Note that a local interference pattern of S on Z can be seen below the hammer.

(a)

(b)

Figure 17

Minor fold patterns. Lines are axial traces. Dashed lines are structure markers. Stippled area is domain VII. The symbols S and Z representing the different minor fold patterns are put on the localities where they were observed.

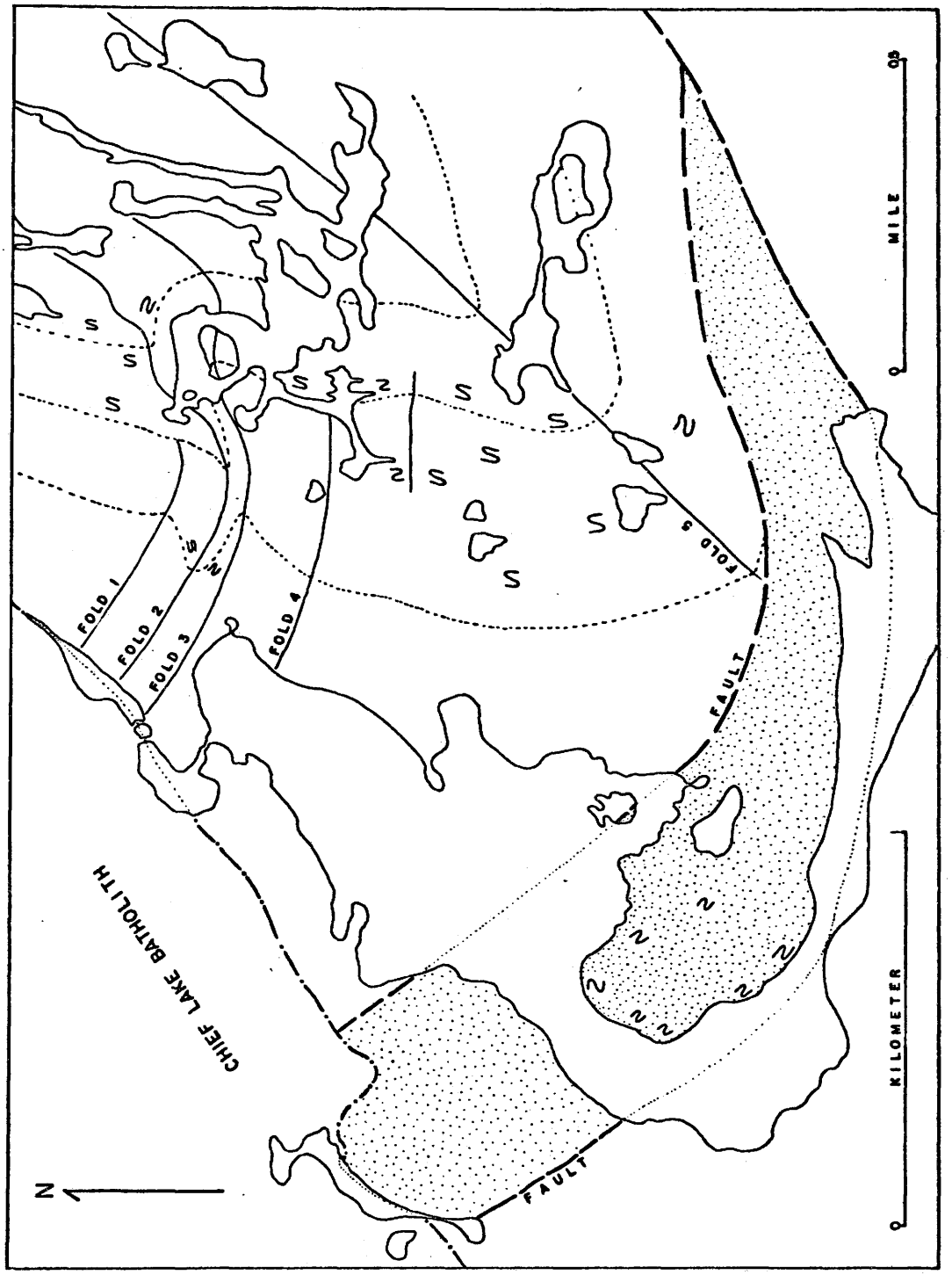
FOLD 1
FOLD 2
FOLD 3
FOLD 4
FOLD 5
FAULT
FAULT
CHIEF LAKE BATHOLITH
N
0
MILE
0
KILOMETER

The usefulness of S and Z fold-forms on outcrop patterns is not questionable in the map area, since all the limbs of folds dip moderately to steeply.

IV. GEOMETRY OF MACROSCOPIC FOLDS

Five macroscopic folds have been defined in the map area. They were subjected to second folding, so that their axial traces are curved except fold 5 which is intersected by a fault to the south. The curved axial traces of folds 1-4 are more or less subparallel and extend to the west-northwest until they are truncated by the batholith which cuts the Grenville province rocks in a northeasterly direction (Figures 2 and 18). Folds 1 and 4 extend easterly and then disappear when they reach the relatively competent layers of pink K-feldspar gneiss; whereas the northeastern limit of folds 2, 3, and 5 are not certain, since their axial traces extend parallel to the regional gneissosity, and the hinge zones of these folds to the northeast might have been sheared out into parallel layerings.

So far as the axial traces can be observed, the macroscopic folds vary their tightnesses from close to gentle (Fleuty, 1964, pp. 470-471). The first folds were subjected to a second folding which caused the axial surfaces of first folds to form an open antiform pattern (angle between surface inclination measured at the inflexion points on the

Figure 18

Macroscopic folds and subdivision of domains III and IV.

Stippled is the area subjected to later local rotation.

Roman numerals represent different domains.

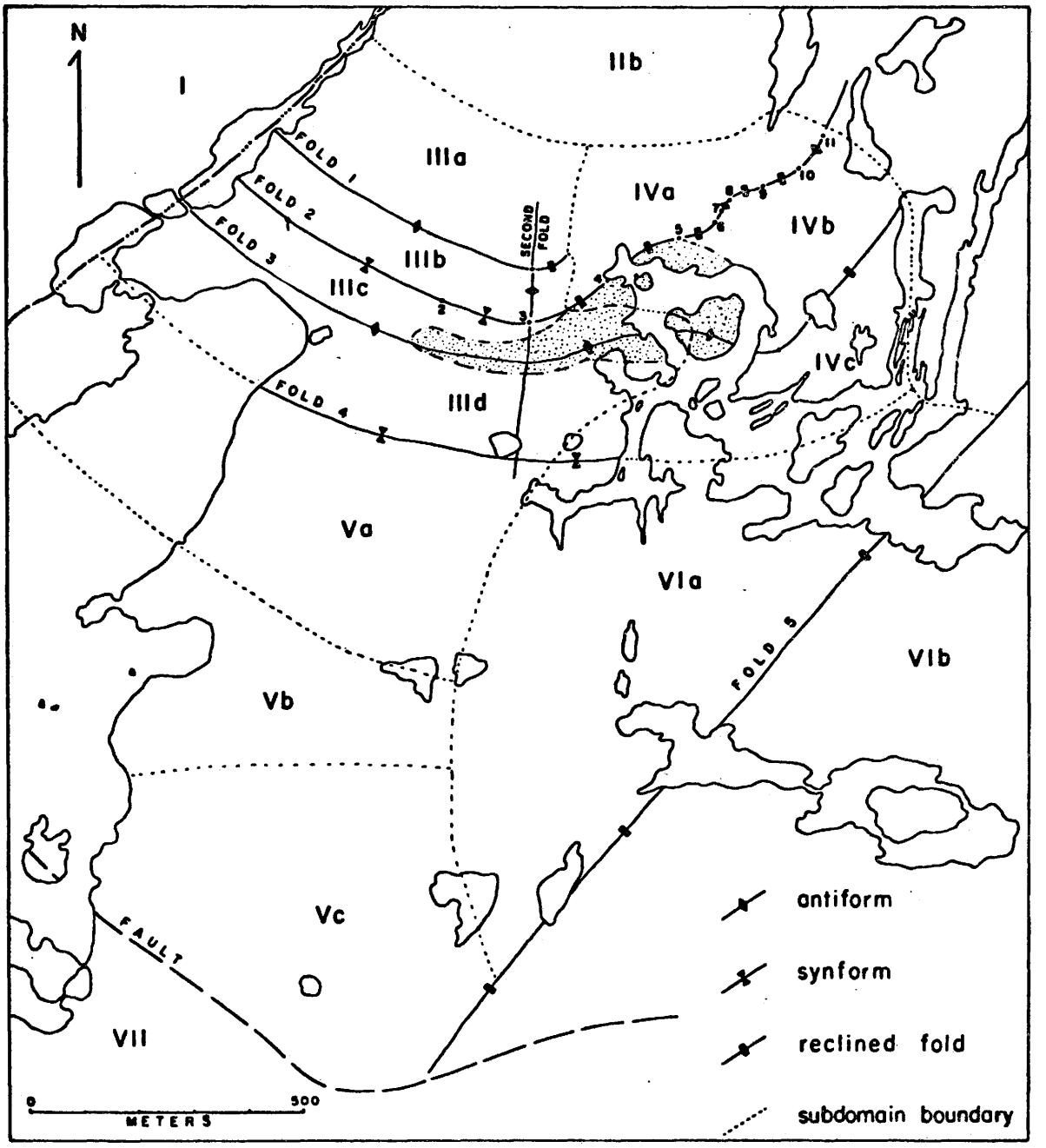
N
I
IIb
IIIa
IIIb
IIIc
IIId
IVa
IVb
IVc
Va
Vb
Vc
VII
VIa
VIb
FOLD 1
FOLD 2
FOLD 3
FOLD 4
FOLD 5
SECOND FOLD
FAULT
0
500
METERS
antiform
synform
reclined fold
subdomain boundary

map is about 110°) with its crest towards the south. The axial trace of the second fold strikes 005 degrees.

The curvatures of the two faults across Brodill Lake are quite similar to those of the axial traces of first folds (Figures 2 and 18). It seems likely that the fault planes were also subjected to the same second folding. If this is true, the axial trace of the second fold would turn in direction from 185° to 198° towards the fault.

Fold 1

Fold 1 comprises subdomain IIIa as its north limb and subdomain IIIb as its south limb (Figure 18). The Sg-poles as well as the associated mineral lineations on the two limbs are plotted in Figure 19(a). A great-circle girdle passing through the Sg-poles is centered on the fold axis which parallels the dominant trend of mineral lineations. Hence $B=b=L_1$ (Wilson, 1967), which is oriented at 154 degrees and plunges 60 degrees. The axial trace is curved; it strikes 124 degrees at its western border and runs east-southeast. The axial trace strikes 085° near its maximum curvature and then turns its direction to the east-northeast. The dip of the axial surface varies in decreasing order from 71° at its western border to 60° at its east end

Figure 19

Geometry of fold 1. Solid dots, L_1; solid triangles, Sg-poles; cross, fold axis; heavy curve, locus of axial-surface-poles; A, antiform; R, reclined fold; AS, axial surface; roman numerals, subdomain names.

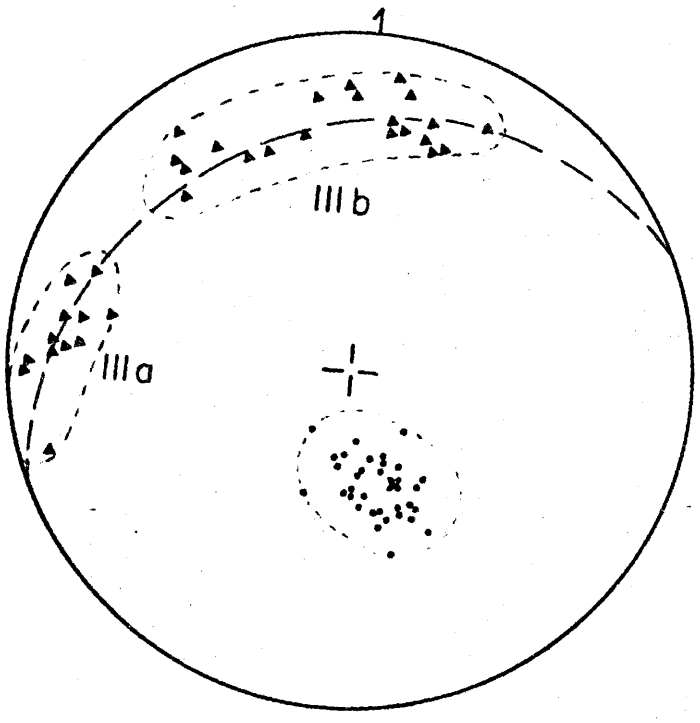

a

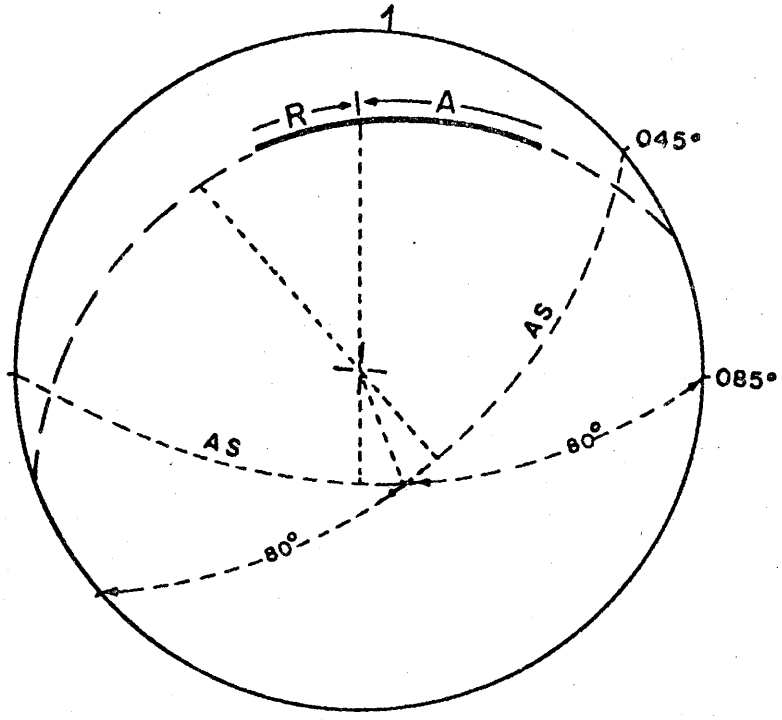

b

where the fold disappears. The locus of the poles to the axial surface is shown in Figure 19(b). Thus, west of the second fold axis, fold 1 is a steeply inclined, moderately to steeply plunging antiform whereas the eastern section of the fold is a moderately to steeply inclined reclined fold (Fleuty, 1964).

Fold 2

The axial trace of fold 2 is nearly parallel to that of fold 1 and is located about 110 meters to the south. If the axial surface of the second fold is used to divide fold 2 into two sections, then the western section of fold 2 comprises most of the rocks in subdomains IIIb and IIIc whereas the eastern section comprises not only the whole of subdomains IVa and IVb but also the eastern part of subdomains IIIb and IIIc. Figure 20(a) shows that the Sg-poles of the western section of fold 2 form a great-circle girdle centered on the mean concentration of mineral lineations plunging 60° at 156°. Hence, $B=b=L_1$ no matter how the axial surface changes. The axial trace of fold 2 measured at point 1 in Figure 18 strikes 125°, so the "normal" axial surface in the ideal case should dip 73° to the southwest. Similarly, in the ideal case the axial surface strikes 111° and 101°, and dips 68° and 62° to the southwest at points 2 and 3, respectively.

Figure 20

Geometry of fold 2. Solid dots, L_1; cross, fold axis; AS, axial surface; S, synform; R, reclined fold; A, antiform; numbers, measurement numbers in Figure 18; (a) and (b), western section; (c) and (d), eastern section; heavy lines, loci of axial-surface-poles. Solid triangles in (a) are Sg-poles in subdomain IIIb while those in (c) are Sg-poles in subdomain IVa. Open triangles in (a) are Sg-poles in subdomain IIIc while those in (c) are Sg-poles in subdomain IVb. (e), combined loci of axial-surface-poles in (b) and (d) show the orientation of the second fold axis.

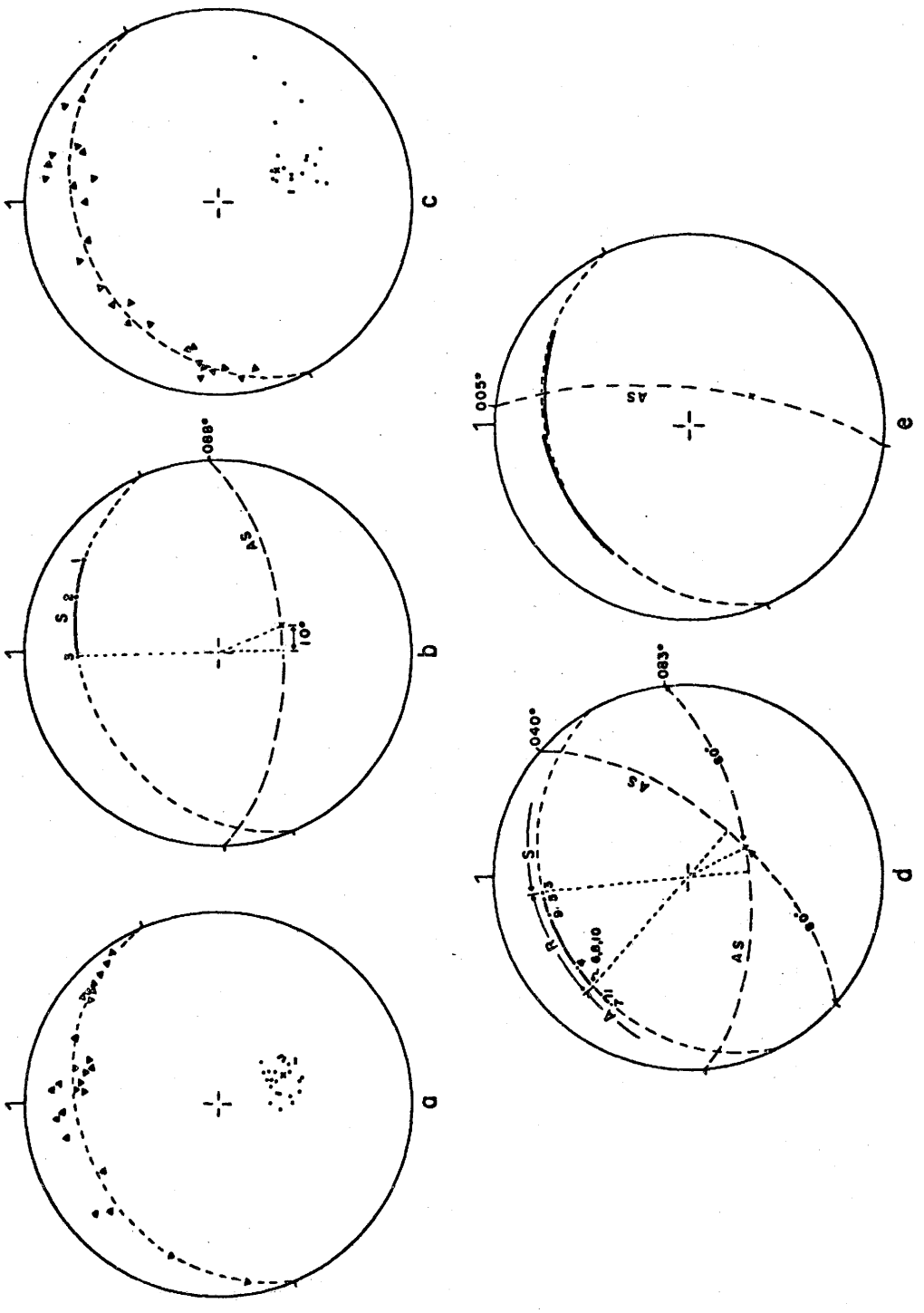
1
a
1
c
088°
AS
S
10°
1
b
1 005°
e
040°
083°
AS
S
AS
d

The locus of poles to axial surfaces for the western section of fold 2 is shown in Figure 20(b). Since the fold axis always has a pitch of less than 80° on the axial surface, the western section of fold 2 is a steeply inclined, moderately to steeply plunging synform.

The eastern section of fold 2 is of much more interest. The axial trace of the fold has four inflexion points as it extends northeast (Figure 18). As noted before, subdomain IVb comprises several type 3 mesoscopic folds and the mineral lineations in the subdomain are deformed. Therefore, in the geometric analysis of the eastern section of fold 2, only those structural data collected in the vicinity of the axial trace are used. The Sg-poles and associated mineral lineations are plotted on Figure 20(c). The fold axis plunges 62° in 152°-direction, around which mineral lineations are scattered, although there is a tendency for lineations to be rotated eastwards (discussed later). In general, the fold axis parallels the mineral lineations. With a fixed fold axis, the axial surface must change its dip while changing its strike. The locus of the poles to the deformed axial surface in the ideal case should lie on the same great circle as Sg-poles, which is plotted on Figure 20(d). In the diagram, the region of reclined fold (R) and antiform (A) are shown. At point 3 in Figure 18, the axial surface strikes 083° and dips 63° to the south,

then the axial trace extends northeast until it reaches point 4 where the axial surface strikes 050° and dips 62° to the southeast. From point 4 on, the axial trace extends by first turning its direction to the east at point 5 and then turning to the north-northeast at point 7. Failing to maintain a straight line, the axial trace once again turns to the east-northeast from point 8 and finally turns to the direction around 036° at point 11. The poles of the deformed axial surface at each point in the ideal case are shown in Figure 20(d).

Based on the above description, the western section of fold 2 is a synform (between points 1 and 3), the section between points 3 and 10 (except the short part of antiform between points 6 and 8) is a reclined fold, and finally the northeast of point 10 is an antiform. Although fold 2 appears as variable forms at different places, its axis maintains the same orientation. This kind of fold is here called a "composite fold". The composite fold probably resulted from coaxial repeated folding, since the axial surface of first fold forms a cylindrical fold around the axis of second fold, which is identical with that of first fold. It is also possible that the composite fold is simply a product of an inherited plane subjected to a strong uniaxial flow deformation (discussed later).

The orientation normal to the plane containing the axial-surface-poles of the first fold (i.e. fold 2 in this case) is the axis of the second fold (Figures 20d and 20e), which is also parallel to the regional mineral lineations. The axial trace of the second fold measured on the map is oriented at 005° and so in the ideal case the axial plane* dips 74° to the east (Figure 20e).

Fold 3

Fold 3 lies to the south of fold 2; the axial traces of the two folds are separated by a distance varying from 50 to 280 meters (Figure 18). There seems to have been a later rotation in the core of fold 3 along the boundary between subdomains IIIc and IIId, where the mineral lineations tend to plunge to the east-southeast, different from those in the surrounding areas. The structural elements of fold 3 in subdomains IVb and IVc are not subjected to geometric analysis, since most of the mineral lineations were deformed. In subdomains IIIc and IIId, the axial trace of the second fold is used to divide fold 3 into two sections. The Sg-poles and mineral lineations of the western and the eastern sections of fold 3 are plotted on Figures 21(a) and 21(b), respectively. The fold axis of the western section plunges 54° in

*The topographic relief in the area is rather low, so the strike of axial plane is almost the same as axial trace.

Figure 21

Geometry of fold 3. Triangles, Sg-poles. Other symbols are the same as those in Figure 20.

(a) Western section.

(b) Eastern section.

(c) Loci of axial-surface-poles.

(d) Non-rotated area.

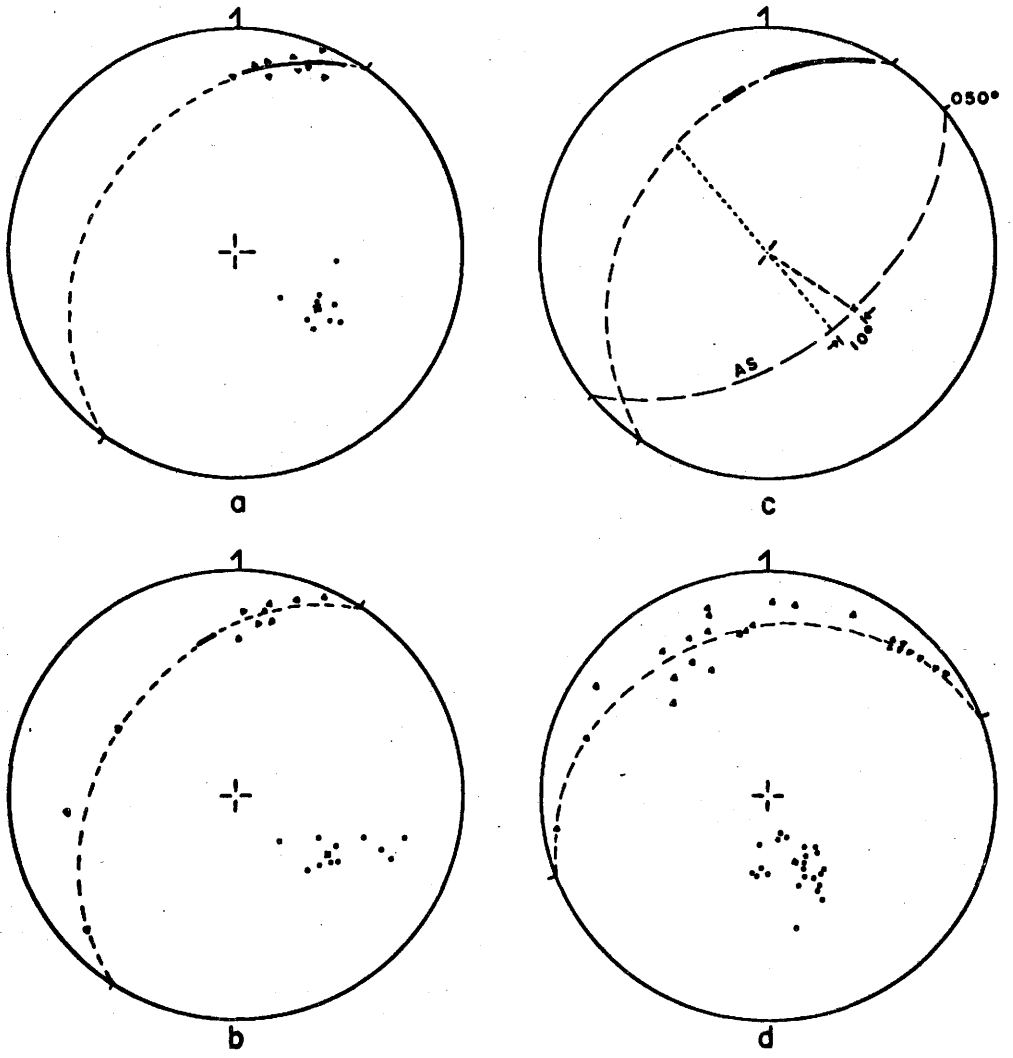
1
a
1
050°
AS
10°
c
1
b
1
d

124°-direction while that of the eastern section plunges 50° in 120°-direction. In each diagram, the fold axis is very close to the dominant trend of mineral lineations, indicating that all the linear structures are parallel and were rotated to the same orientation.

The locus of the poles to the deformed axial surface of fold 3 in subdomains IIIc and IIId are shown by the heavy line in Figures 21(a) and 21(b); all of them fall in the antiform region (Figure 21c).

In contrast to the rotated features, the structural data in the remaining parts of subdomains IIIc and IIId are plotted in Figure 21(d) which shows that the linear structures are oriented the same as those of the surrounding subdomains. The fold axis plunges 64° in 158°-direction, and is parallel to the dominant trend of mineral lineations.

Fold 4

Fold 4 starts from the shore of Brodill Lake and disappears after extending in an easterly direction for half a mile (800 meters). The axial trace is about 190 meters south of that of fold 3. In the stereogram of Figure 22(a), the Sg-poles of both limbs of fold 4 are distributed around a great circle which is centered on the fold axis and the dominant trend of L_1. The locus of the poles to the slightly-deformed axial surface is shown by the heavy line. Fold 4 is a steeply

Figure 22

Macroscopic geometries of folds 4(a) and 5(b).

Small solid triangles are Sg-poles; other symbols are the same as those in Figure 20.

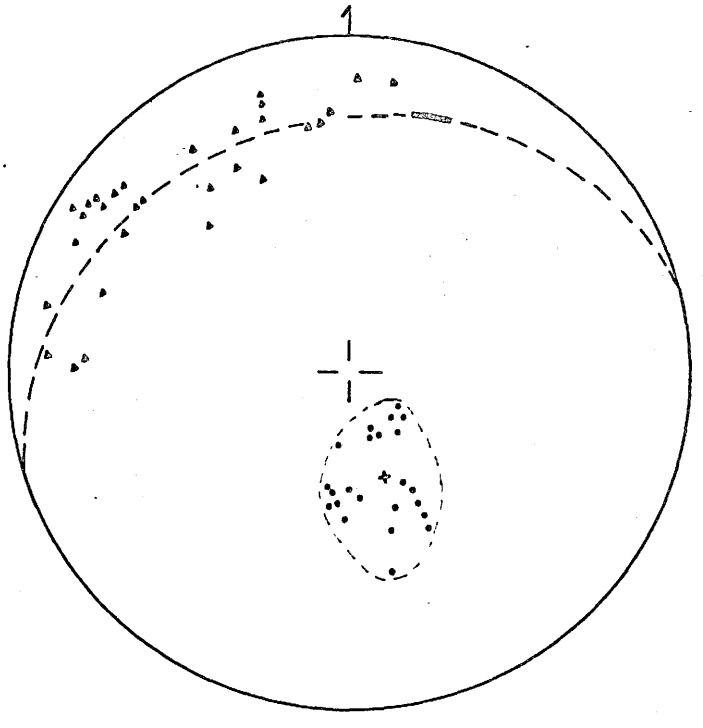

a

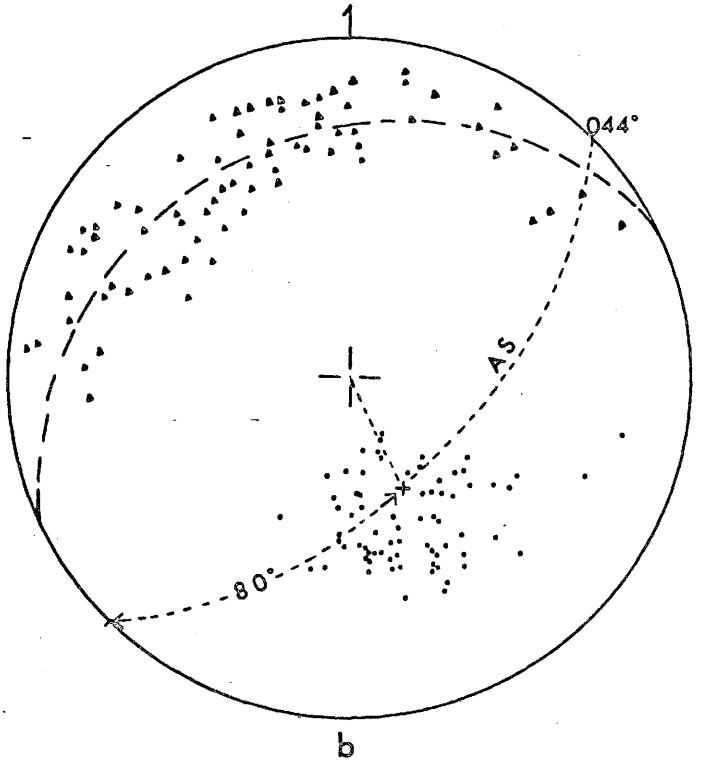

b

inclined, steeply plunging synform whose axis plunges 64° in 163°-direction.

Fold 5

Fold 5 is the major fold in the map area. The axial trace strikes 044° and shows no deformation. To the southwest, the fold is intersected by a fault. The fold axis plunges 61° at 154° and has a pitch of 80° on the axial plane (Figure 22b). Therefore, the steeply inclined fold may be either reclined or antiformal.

Discussion of Macroscopic Fold

When all the loci of the poles to the deformed axial surfaces of the five macroscopic folds are plotted on Figure 23, it is clear that the loci of folds 1, 4, and 5 are almost parallel to that of fold 2. Therefore, a single great circle can well represent those loci. This great circle, centered on point A (axes of folds 1, 2, and 5), intersects the locus of the axial-surface-poles of fold 3 at point R which is oriented at 351° and plunges 28°. It seems reasonable to conclude that the axial surface as well as limbs and fold axis of fold 3 might have been rotated in an easterly direction from their original position (such as A for the fold axis) around an axis of R-direction.

Figure 23

Rotation of fold 3. Heavy lines, loci of axial-surface-poles; F1, fold 1, and so on. Loci of axial-surface-poles of folds 1, 2, 4, and 5 almost lie on a common great circle which intersects that of fold 3 at point R. As R is moved to the horizontal position in its plunging direction, points A and 3 are rotated to points A' and 3', respectively. The angle between the two orientations of points A' and 3' is 19°.

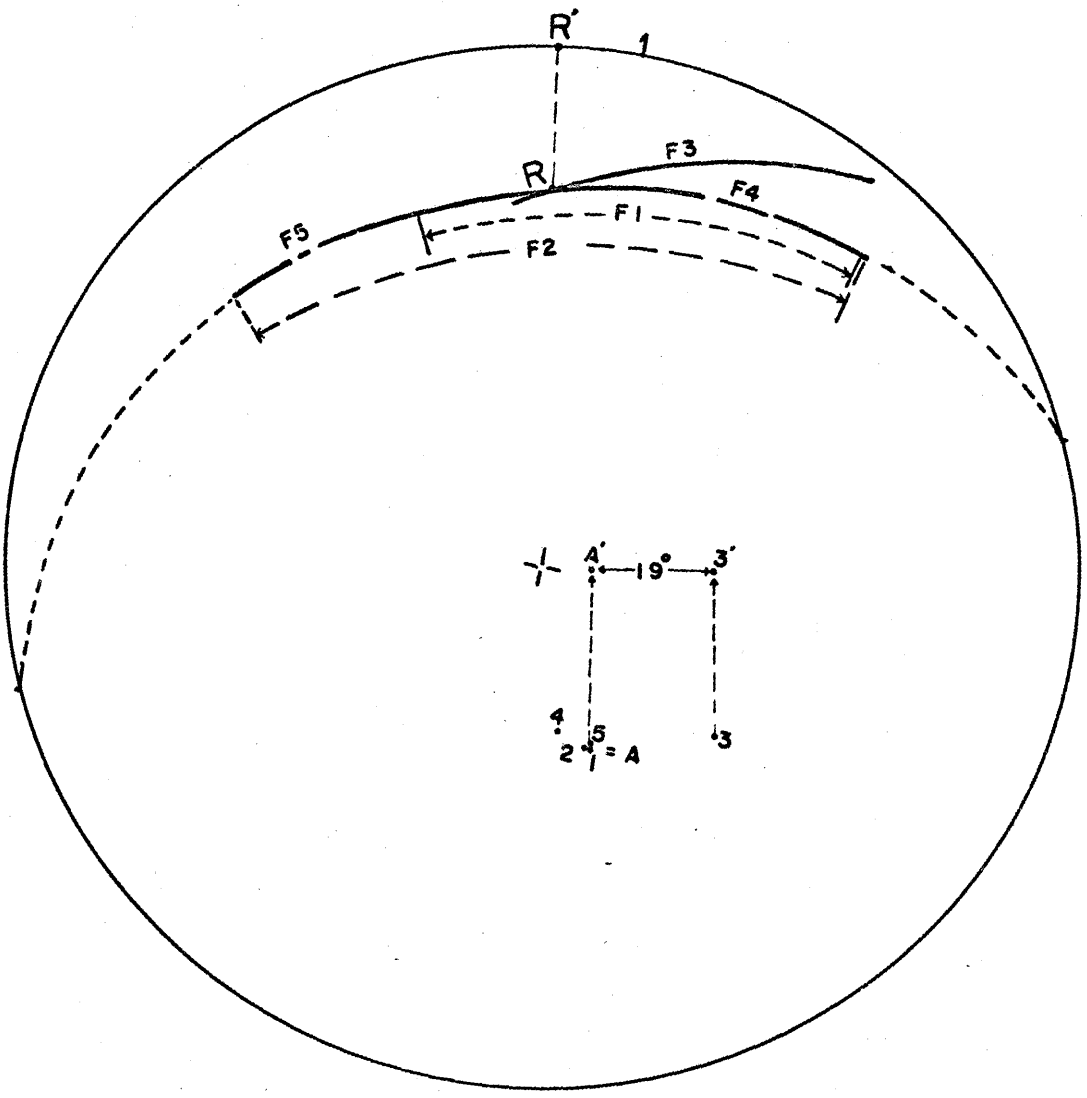
R'
1
R
F3
F4
F5
F1
F2
A'
19°
3'
4
5
2
1 = A
3

The angle that fold 3 rotated around R-direction can be found by the following techniques: first, rotate R to a horizontal position in its plunge direction; at the same time, points A and 3 (not curve 3) are moved to points A' and 3', respectively; and second, measure the angle between points A' and 3'. In Figure 23, the angle measured is 19°; that is, fold 3 rotated in an easterly direction around an axis of R-direction with an angle of 19°.

The geometries of macroscopic folds and refolds in Sg and mineral lineations are the same as that of the mesoscopic folds of type 1. The diagram in Figure 23 is actually the same as that in Figure 11.

V. PRINCIPAL STRAIN DIRECTIONS

According to the symmetry principle, the symmetry of the tectonite fabric of a rock reflects the symmetry of the deformation in the rock. Hence, the structural elements recorded in the field can be arranged in different ways, from which certain symmetries of tectonite fabrics may be used to locate the principal directions of strain (Flinn, 1965).

The deformation of rocks has been treated in terms of finite homogeneous strain by several people (Brace, 1961; Flinn, 1962, 1965; Turner and Weiss, 1963; Ramsay, 1967). The finite homo-

geneous strain which a rock has suffered is conveniently represented by the shape and orientation of the constant-volume deformation ellipsoid, which may represent a portion of the rock which at the start of the deformation was spherical (Flinn, 1965, p. 36). The axes of the deformation ellipsoid are labelled $Z>Y>X$, referring to the maximum, intermediate, and least principal strain directions.

Domain I

The macroscopic geometry of S_f and L_1 in domain I shows a monoclinic (nearly orthorhombic) symmetry (Figure 6), with a symmetry plane containing the S_f-poles and normal to the maximum concentration of mineral lineations. The fabric symmetry may represent what Flinn (1965) called "L>S tectonite ($\infty > k' > 1$)*" with constriction-shaped orthorhombic ellipsoid ($Z \gg Y > X$), of which the axes are oriented so that the longest axis (Z) of the ellipsoid lies parallel to L_1 in the fabric, and the longest and the intermediate axes lie on a plane parallel to the foliation S_f. The X-axis therefore parallels the dominant trend of S_f-poles.

Domains II-VIII

The orthorhombic macroscopic symmetry of Sg and L_1 in domains II-VIII (Figure 8a) can also be related to a triaxial deformation ellipsoid of the type $Z \gg Y > X$; i.e. the penetrative L_1 was

* Flinn (1965b) defined the k'-value as $a=b^{k'}$, where $a=\frac{Z}{Y}$ and $b=\frac{Y}{X}$. Hence, $k' = \log a / \log b$.

active, formed parallel to the Z-axis, but the Sg was passive, rotated normal to the X-axis (Flinn, 1962) during the final strong deformation. The dominant orientation of passive Sg-poles (i.e. the assumed X-direction which parallels m_1 : m_2 in Figure 8) plunges 36° in 329°-direction while the maximum concentration of mineral lineations is oriented at 153° and plunges 54°. The Y-direction is normal to the symmetry plane m_2 containing the maximum concentration of L_1 and the dominant trend of Sg-poles (Figure 8a).

Folds of Type 1 and Type 2

Folds of type 1, with fold axes parallel to the penetrative mineral lineation (L_1) and the locus of axial-surface-poles lying on a plane normal to L_1, are found on both mesoscopic and macroscopic scales. The geometry of type 2 folds is similar to that of type 1 mesoscopic folds*; and both types of mesoscopic folds are formed in both the batholith and the Grenville province rocks. The geometry of these folds is compatible with a finite homogeneous strain imposed upon the previously folded rocks in a type of uniaxially elongated

---

* i.e. elongation of type 2 fold is parallel to the fold axis of type 1 fold, while the axial plane containing the long axis of the elliptical outcrop of type 2 fold is equivalent to the axial surface of type 1 fold.

ellipsoid ($Z \gg Y = X$, or $k' = \infty$ as defined by Flinn, 1962 and 1965b); all inherited linear structures (such as fold axes) are rotated to parallel the Z-axis (i.e. the orientation of the penetrative mineral lineations), and all inherited planar elements (such as Sg and axial surface) also are rotated to contain the Z-axis, so that the poles of the rotated planar elements may randomly lie on the X-Y plane (Flinn, 1962). Whether the superimposed folds of macroscopic scale (e.g. the second fold in Figure 18) were formed before or at the time of the batholith intrusion is not certain. The fold form might have been modified during the final homogeneous deformation, since during the deformation a previously-folded layer would rotate bodily so that the fold axis and the axial surface approached the longest axis (Z) of the deformation ellipsoid and the layer might thicken or thin and might fold up further or unfold about the same axis (Flinn, 1962).

Type 3 Fold

The mesoscopic folds of type 3 may be the youngest structures of regional significance in the map area, since the regional penetrative mineral lineations were deformed around the hinges of the folds. The axial plane, which contains the flow direction a and the fold axis, is perpendicular to the regional X-direction although a certain deviation exists.

The folds of type 3 were characterized by an active axial plane, formed during a later stage of the final deformation. The mineral lineation that developed at an earlier stage of the deformation was involved passively in the slip folding. Most of the deformed lineation loci do not pass through Z, probably because the folds were rotated bodily so that the fold axes moved slightly toward Z and thus made the loci of deformed lineations depart from Z.

Normally, during a finite homogeneous strain no fold can be generated, because straight lines must remain straight. However, if there is a competence difference between the layers which happen to be oriented in such a way that they contain the maximum stress axis (or the least strain axis X), the layers may be expected to buckle. As soon as buckling is present it will be acted by the homogeneous strain to form slip folds and further folding will be a mixture of similar folding due to homogeneous strain and concentric folding due to the buckling (Flinn, 1962, p. 424). In general, during deformation the homogeneous strain components are arranged so that the maximum shortening (X) is perpendicular to the shear plane (axial plane), and the fold axis gradually moves towards the Z-axis but the structure remains cylindrical (Ramsay, 1967, p. 481). In the map area, all the folds of type 3 are found in the hinge zones of macroscopic folds or at

places where the layers contained the X-direction before being folded (Figure 24). Most of the type 3 folds show a deformed lineation belonging to a similar-fold model and the buckling component is of little significance. Ramsay (1967, p. 482) explained this as follows: "If the shear component is strongly developed and entirely later than the buckling component, the deformed lineation locus develops a continuous geometric form characteristic of true similar folds".

Based on the above discussion, the processes of the formation of type 3 folds can be interpreted as follows:

1) During a later stage of the final deformation (when the penetrative mineral lineations were formed), certain small buckling folds would be developed in the layers containing the X-direction (such as those in subdomain IVb). The newly generated axial planes would be perpendicular to both the X-direction and the layers being folded, while the fold axes might be variable in the Y-Z plane depending on the attitude of the plane before folding, i.e. the fold axis would be parallel to the dip-direction of the plane being folded.

2) As soon as buckling was present, it would be acted on by the homogeneous strain to form a slip fold. The flow (slip) direction a (shown by open arrow on Figure 24b), as obtained from the analysis of deformed mineral lineations, initially paralleled the

Figure 24

a) A layer ABCD containing the X-direction before being folded. X, principal shortening direction; Z, principal elongation direction; L_1, mineral lineation.

b) After folding, the locus of the deformed mineral lineation lies on a plane (stippled).

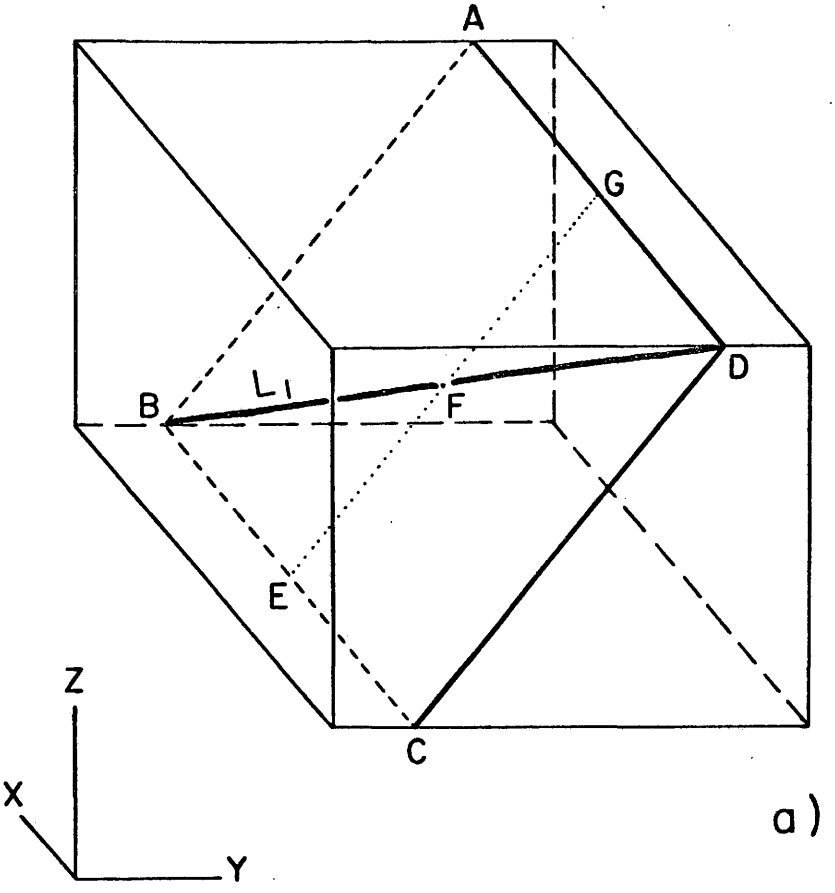

a)

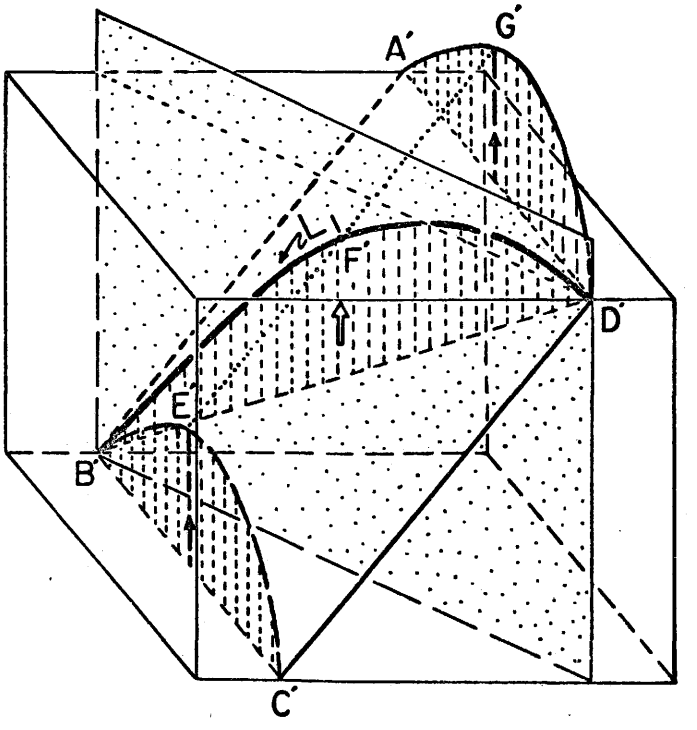

b)

Z-direction. The axial planes maintained an attitude normal to the X-direction while the fold axes still had the freedom of orientation on the Y-Z plane.

3) As progressive deformation continued, the folds would rotate bodily so that the axes would move toward the longest axis (Z) of the deformation ellipsoid; consequently, the flow direction a recorded on each fold would move accordingly apart from the Z-direction, and the angle each a rotated off the Z-axis would be the same as the angle the fold axis moved toward the Z-axis. The axial planes at this stage still would maintain an attitude parallel to the Y-Z plane. In the case of the map area, the flow directions (a) of type 3 folds are closer to the Z-axis (i.e. orientation of regional penetrative linear structures) than the fold axes, indicating that the final deformation had ended before the fold axes of type 3 folds could be moved to parallel the longest axis (Z) of the deformation ellipsoid.

Type 4 Fold

The fold of type 4 is but a single fold found in the map area and thus has no regional significance. The fold axis and the axial plane have no relation to the principal strain directions discussed above. It is clear that the fold was formed by a local strain after the final regional deformation.

Discussion on Homogeneous and Inhomogeneous Deformation

By definition, in homogeneous deformation a straight line remains straight and parallel lines remain parallel after deformation (Ramsay, 1967); hence in theory no fold or boudins can be generated. All that can happen is the opening or further closing of previously formed folds and the passive rotation of inherited planes and structures (Flinn, 1962). However, from the structural studies of the map area, a new concept of deformation in a three-dimensional, constantly-oriented stress field is derived in which the deformation may be either homogeneous or inhomogeneous or both, depending on the competence difference between layers (Ramberg, 1959 and 1960), and also on the relationship between the attitude of layers before deformation and the principal compression direction.

As has been mentioned earlier, all the mesoscopic folds of type 3 in the map area are found only at the places where the layers were parallel or subparallel to the compression direction (the X-direction) before being folded. In subdomain IVb, the dominant trend of the layers (Sg), striking 123° and dipping 70° to the southwest, is parallel to the compression component of regional strain field, and so the rocks in this subdomain were wholly deformed into many folds similar to that of type 3. In addition, numerous mesoscopic folds of

type 3 are found occurring along the hinge zone of the major macroscopic fold (fold 5 in Figure 18) in the area, although many of the individual fold blocks (mesoscopic folds) have been moved due to later local rotation. This suggests that in a constantly-oriented three-dimensional stress field, rock layers with different competence may be subjected to an inhomogeneous deformation in the places where the layers parallel or subparallel the compression component, while the layers normal or subnormal to the compression may show no inhomogeneous deformation.

In the case of the map area, because the subdomain IVb is small, the deformation of the whole area studied is regionally homogeneous with locally inhomogeneous small folds (mostly occurring in subdomain IVb and the hinge zones of macroscopic folds), and shows that the principal strain directions of the inhomogeneous deformation are the same as those of the regional homogeneous strain, since the axial planes of type 3 folds are perpendicular to the X-direction and the $\underline{a}$ directions are very close to the Z-direction. However, if the previous layers of the map area had been all parallel to those in subdomain IVb (i.e. parallel to the compression), then the whole area might have been showed inhomogeneous deformation by producing numerous new folds of type 3 after being subjected to three-dimensional stresses. On the other hand, if no previous layers

parallel or subparallel to the compression (X-direction) and no previous fold having layers parallel to the compression in its hinge zone had occurred, then the area would have showed no inhomogeneous deformation after being subjected to the same stresses.

The structural geometries of the folds of type 1 (Figure 11) show that the fabric symmetries of the folds can be compared with the deformation ellipsoid of type $Z \gg Y = X$, in which inherited planar element (e.g. axial surface or Sg) lies parallel to the Z-direction, and the pole of the plane has complete freedom of orientation on the X-Y plane. Accordingly, an inherited plane might be passively folded around the Z-axis during the deformation and produce a strain geometry similar to the deformation ellipsoid of type $Z \gg Y = X$, and thus the deformation is inhomogeneous. On the other hand, it is also possible as noted before that the folds of type 1 might be inherited folds which were moved bodily so that the fold axes rotated towards the Z-axis from their original positions during the final regional deformation, and thus the deformation is homogeneous. Therefore, type 1 folds may belong to either homogeneous or inhomogeneous deformation, but the principal strain directions derived for both types of deformation are the same.

Based on the above argument, rock deformation may be either homogeneous or inhomogeneous from place to place in a region such as the map area; the principal strain directions derived for both deformations are identical. Therefore, the formation of type 3 folds and, probably, part of type 1 folds formed by inhomogeneous deformation can also be compared with the deformation ellipsoid.

Summary of Principal Strain Directions

The different types of deformation ellipsoid as compared to the fabric symmetries of different structural elements in the map area are listed in Table IV. Among the different types of deformation, active S_f is homogeneous whereas type 3 fold is inhomogeneous with a slight component of homogeneous strain, since the fold axes have moved slightly towards the Z-axis and consequently $\underline{a}$ directions moved slightly apart from the Z-direction. On the other hand, the deformations of Sg and folds of types 1 and 2 may be inhomogeneous if the rock layers were previously planar, or homogeneous if the rocks had been already folded before the final deformation.

Table IV. Comparison of deformation ellipsoid with different structural fabric symmetries

Structural element		Type of deformation ellipsoid
Types 1 & 2 folds	Active L_1	$Z \gg Y = X$ ($k' = \infty$)
Passive Sg (domains II-VIII) Active S_f (domain I)		$Z \gg Y > X$ ($\infty > k' > 1$)
Type 3 fold	Passive L_1 defining $\underline{a}$	$Z > Y > X$ ($k' = 1$)

In general, the principal axes of strain for the fabric symmetries of different structural elements are almost coincident (Figure 25), suggesting that whether the deformation was homogeneous or not, the principal strain directions were constantly oriented throughout the final regional deformation, wherein the Z-axis parallels active L_1, passive type 1 fold axes, elongations of type 2 folds, and original $\underline{a}$ directions of type 3 folds; while the X-axis is parallel to the dominant trend of Sg-poles, maximum concentration of S_f-poles, and the axial-plane-poles of type 3 folds. The direction

Figure 25

Principal directions of equal-volume strain ellipsoids.

(a) Uniaxial prolate type $Z \gg Y = X$ ($k' = \infty$). Z-direction parallels fold axes and L_1. 1, mesoscopic folds of types 1 and 2; 2, macroscopic folds of type 1.

(b) Constriction type $Z \gg Y > X$ ($\infty > k' > 1$). Z-direction parallels L_1; X-direction is normal to dominant trend of Sg(3) and maximum concentration of S_f(4).

(c) Plane-strain type $Z > Y > X$ ($k' = 1$). Z-direction subparallels flow directions and X-direction is normal to axial planes of type 3 folds (5).

(d) Coincidence of the principal strain axes of different types.

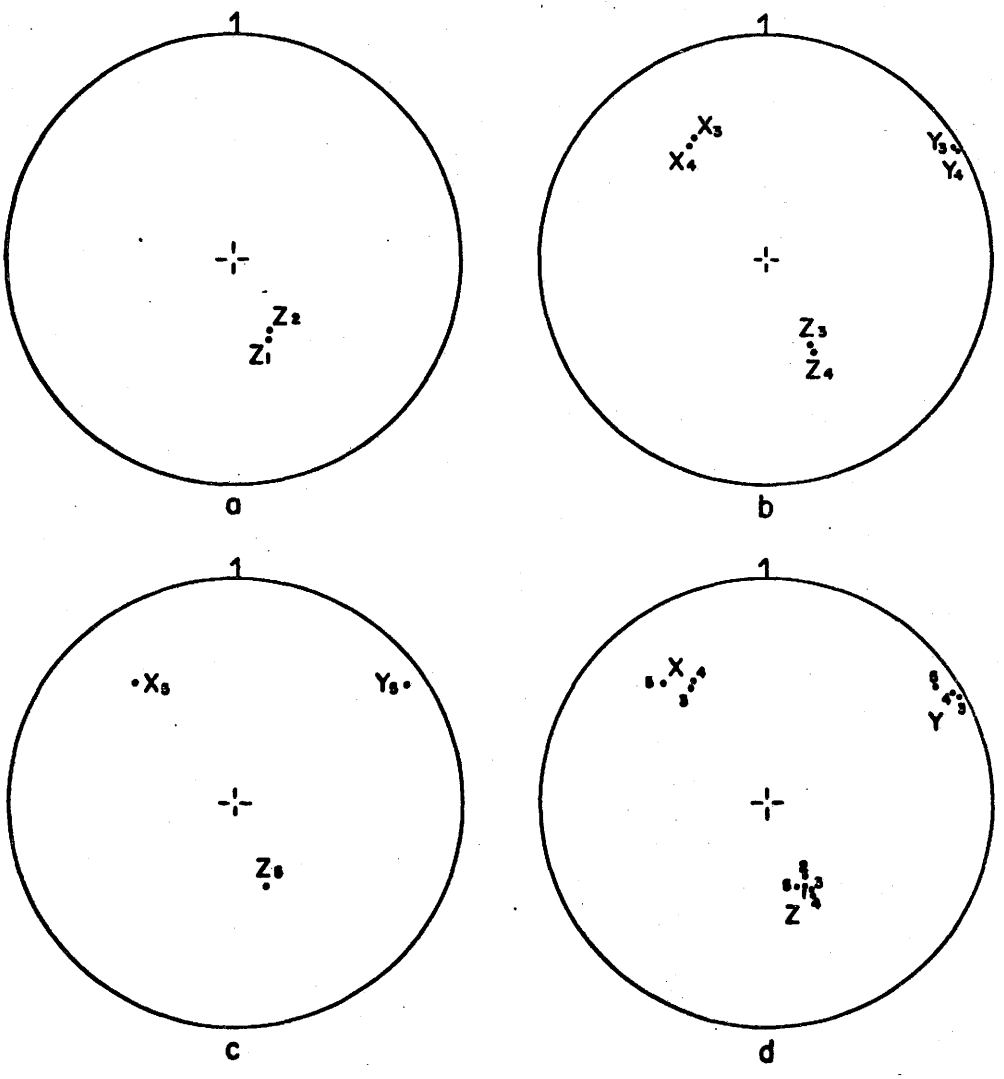
1
Z2
Z1
a
1
X3
X4
Y3
Y4
Z3
Z4
b
1
X5
Y5
Z5
c
1
X
Y
Z
d

of maximum elongation (Z) plunges moderately to the south-southeast and that of maximum shortening (X) generally plunges to the northwest.

Because type 1 folds in the batholith are penetrated by S_f, and thus the formation of the folds was earlier than that of S_f; also because type 3 folds were formed at a later stage of the final deformation (pp. 84-86), the constantly-oriented principal strain axes of the final regional deformation are assigned to as initiated from type $Z \gg Y = X$ ($k' = \infty$), passing through type $Z \gg Y > X$ ($\infty > k' > 1$), to type $Z > Y > X$ ($k' = 1$). If these are compared to Flinn's (1965) L-S fabric system, then the tectonites were changed from L (uniaxial prolate type) through $L > S$ (constriction type) to $L \approx S$ (plane-strain type) during the progressive deformation (see also Table IV).

VI. DYNAMIC ANALYSIS

Henderson (1967) compared the similarity between the internal fabric symmetry of salt domes and the fabric symmetry of lineated rocks in a larger area to the southwest of the map area, and concluded that the "dominant flow direction was parallel to the regional trend of mineral lineation". This conclusion is also

reached in the present study. The strong parallelism of the regional mineral lineations and the passive fold axes (type 1 folds) found in the recrystallized zone including both the southeastern portion of the batholith and the whole Grenville province in the map area, indicates that strong flowage movement prevailed in the recrystallized zone during the final regional deformation, which rotated all the inherited linear structures (such as fold axes) to parallel the flow direction and simultaneously produced the penetrative mineral lineations.

The cataclastic zone is a wide shear zone striking parallel to the regional penetrative foliation (S_f). The mineral lineations developed on the shear plane in the cataclastic zone are the same as all regional penetrative linear structures which plunge moderately to the south-southeast. In addition, the cataclastic zone is a metamorphic break with high-grade rocks on the southeastern side. Therefore, the flow movement was upwards to the northwest.

It has been remarked that the slip folds of type 3 might have been developed by a process of progressive inhomogeneous contraction at a later stage of the finite homogeneous strain. The shear component of the fold was, in fact, the result of the inhomogeneity in the shortening of certain layers, and thus the slip direction a

generally was lying close to the principal elongation direction (the Z-axis of deformation), and the axial plane was perpendicular to the principal compressive strain. The prominent northeast-striking and southeast-dipping foliation (S_f) which parallels the axial plane of active folding, might, in part, result from the same compressive strain.

CHAPTER 5

TECTONIC SYNTHESIS

The origin of most rocks in the "Grenville province" is not certain. However, from the evidence that numerous lit-par-lit injections of mesoscopic as well as macroscopic pegmatite occur along the foliation or banding in quartzo-feldspathic gneiss and laminated quartz amphibolite, a previous metamorphism is assumed to have occurred in the map area, producing the foliae in the metamorphic rocks, along which later igneous materials intruded.

The pegmatite sills were involved in the first generation of folding on both macroscopic and mesoscopic scales, which probably caused not only the production of foliation in pegmatite, parallel to the folded layers, but also formed the congruous parasitic S- and Z-folds. After the folding took place, the two known faults in the map area occurred cutting off the nose of the major fold and transposing a block of rocks (domain VII) containing Z-folds from its original position into contact with a block containing S-folds. The folds of first generation and the two faults were then subjected to a later folding.

About 1,750 m.y. ago (Krogh, in Davis, et al., 1967), the Chief Lake batholith was intruded and truncated the macroscopic superimposed folds. Finally, all the rocks in the map area were subjected to a later regional metamorphism which may represent the so-called "Grenville Orogeny" occurring about 1,000 m.y. ago (Stockwell, 1964; Krogh, 1966). During the final orogenic episode, strong deformation was essentially simultaneous with the regional metamorphism, and the flow movement of high-grade metamorphic rocks prevailed in the recrystallized zone whereas strong shearing occurred in the cataclastic zone.

The rocks northwest of the cataclastic zone belong to the greenschist facies (Henderson, 1967). In the map area, the rocks southeast of the cataclastic zone were completely recrystallized and belong to the sillimanite-muscovite subfacies of amphibolite facies. The sharp increase in metamorphic grade occurs within the cataclastic zone which is about one mile (1,600 meters) wide. In the recrystallized zone, rock deformation shows that finite homogeneous strain was regionally developed with local, simultaneous, mesoscopic folds. During the final regional deformation, all the inherited linear structures were rotated to parallel the strongly-developed regional

mineral lineations, and the higher-grade rocks to the southeast of the cataclastic zone flowed upwards from a greater depth than the rocks to the northwest of the cataclastic zone.

The principal strain axes of the final, regional, progressive deformation were constantly oriented, and are compared with the constant-volume ellipsoids of initial type $Z \gg Y = X$ ($k' = \infty$ or L-tectonite), passing through type $Z \gg Y > X$ ($\infty > k' > 1$ or $L > S$ tectonite), to final type $Z > Y > X$ ($k' = 1$ or $L \approx S$ tectonite); wherein the direction of maximum elongation (Z) plunges moderately to the south-southeast and parallels the regional mineral lineations, the passive fold axes, the elongations of conical folds, and the original flow directions of slip folds; while the direction of maximum shortening (X) generally plunges to the northwest and is normal to the penetrative foliations and the active axial planes of slip folds.

On the basis of the structural data discussed above, the "structural Grenville front" should be put at the western boundary of the cataclastic zone, which is the same line as earlier defined by Henderson (1967) as the western limit of penetrative mineral lineations.

The cataclastic zone was probably a previous fault zone, along which the granitic rocks were intruded to form the Chief Lake batholith 1.75 b.y. ago, and also along which the Grenville province rocks subsequently flowed upwards from a deeper position in the crust.

BIBLIOGRAPHY

Clifford, P.M. et.al. (1957): The development of lineation in complex fold systems. Geol. Mag., vol. 94, pp. 8-10.

Coleman, A.P. (1914): The Pre-Cambrian rocks north of Lake Huron, with special reference to the Sudbury Series. Ontario, Bur. Mines, v. XXIII, pt. 1, pp. 204-236.

Cook, H.C. (1946): Problems of Sudbury Geology. Geol. Surv. Canada, Bull. 3.

Fairbairn, H.W., Hurley, P.M., and Pinson, W.H. (1965): Re-examination of Rb-Sr whole-rock ages of Sudbury, Ontario. Proc. Geol. Assoc. Canada, v. 16, pp. 95-102.

Fleuty, M.J. (1961): The three fold-systems in the metamorphic rocks of upper Glen Orrin, Ross-shire and Inverness-shire. Quart. J. Geol. Soc., v. cxvii, pp. 447-479.

_____ (1964): The description of folds. Proc. Geol. Assoc., v. 75, pt. 4, pp. 461-492.

Flinn, D. (1962): On folding during three-dimensional progressive deformation. Quart. J. Geol. Soc., v. 118, pp. 385-433.

_____ (1965a): On the symmetry principle and the deformation ellipsoid. Geol. Mag., v. 102, pp. 36-45.

Flinn, D. (1965b): Deformation in metamorphism, in "Controls of metamorphism". Geol. J. Spec. Issue No. 1, Oliver & Boyd, Edinb.

Grant, J.A (1964): Rubidium-strontium isochron study of the Grenville front near Lake Timagami, Ontario. Science, v. 146, pp. 1049-1053.

_____, Pearson, W.J., Phemister, T.C., and Thomson, Jas. E. (1962): Broder, Dill, Neelon, and Dryden Townships. Ontario Dept. Mines, Geol. Rept. No. 9.

Henderson, J.R. (1967): Structural and petrologic relations across the Grenville province-Southern province boundary, Sudbury district, Ontario. Unpublished Ph. D. thesis, McMaster University.

Hietanen, A. (1967): On the facies series in various types of metamorphism. J. Geol., v. 75, No. 2, pp. 187-214.

Krogh, T.E. (1966): Whole rock rubidium-strontium studies in the northwest Grenville area of Ontario. Transactions, American Geophys. Union (Abs. 47th Ann. Meeting), v. 47, No. 1, p. 206.

_____ (1967): Rb/Sr chronology of the granitic rocks southeast of Sudbury, Ontario, in Davis, G.L., Hart, S.R., Aldrich, L.T., Krogh, T.E., Munizaga, F., Geochronology. Carnegie Inst. Yearbook 65, 1965-1966.

Paterson, M.S., and Weiss, L.E. (1961): Symmetry concepts in the structural analysis of deformed rocks. Geol. Soc. America Bull., v. 72, pp. 841-882.

Phemister, T.C. (1961): The boundary between the Timiskaming and Grenville subprovinces in the townships of Neelon, Dryden, Dill, and Broder, District of Sudbury. Ontario Dept. Mines Prelim. Rept. 1961-5.

Quirke, T.T. and Collins, W.H. (1930): The disappearance of the Huronian. Geol. Surv. Canada, Mem. 160.

Ramberg, H. (1959): Evolution of ptygmatic folding. Norges Geol. Tidskr., 39, pp. 99-152.

_____ (1960): Relationships between length of arc and thickness of ptygmatically folded veins. Amer. Journ. Sci., 258, 36-46.

Ramsay, J.G. (1960): The deformation of early linear structures in areas of repeated folding. J. Geol., 68, pp. 75-93.

_____ (1962): The geometry and mechanics of formation of similar type folds. J. Geol., 70, pp. 309-327.

_____ (1967): Folding and fracturing of rocks. New York, McGraw-Hill.

Stockwell, C.H. (1964): Fourth report on structural provinces, orogenies, and time-classification of the Canadian Precambrian Shield, in Age determinations and geological studies. Geol. Surv. Canada, Paper 64-17, pt. II, pp. 1-21.

_____ (1965): Map 4-1965, Tectonic map of the Canadian Shield. Geol. Surv. Canada.

Tilton, G.R., Wetherill, G.W., Davis, G.L., and Bass, M.M. (1960): 1000 million-year-old minerals from the Eastern United States and Canada. J. Geophys. Res., v. 65, No. 12, pp. 4173-4179.

Turner, F.J. (1958): Mineral assemblages of individual metamorphic facies. Geol. Soc. America, Mem. 73, pp. 199-237.

_____ and Verhoogen, J. (1960): Igneous and metamorphic petrology, 2nd ed. New York, McGraw-Hill.

_____ and Weiss, L.E. (1963): Structural analysis of metamorphic tectonite. New York, McGraw-Hill.

Weiss, L.E. (1955): Fabric analysis of a triclinic tectonite and its bearing on the geometry of flow in rocks. Am. J. Sci., 253, pp. 223-236.

_____ (1959): Geometry of superimposed folding. Geol. Soc. Am. Bull., 70, pp. 91-106.

Wilson, G. (1967): The geometry of cylindrical and conical folds. Proc. Geol. Assoc., v. 78, pt. 1, pp. 179-210.

Young, G.M. and Church, W.R. (1966): The Huronian system in the Sudbury district and adjoining areas of Ontario, a review. Proc. Geol. Assoc. Canada, v. 17, pp. 65-82.